Durham University

Durham E-Theses

Investigating a potential oncogenic role for AGR2 in pro-survival autophagy

DAN, LUCY

How to cite:

DAN, LUCY (2023) *Investigating a potential oncogenic role for AGR2 in pro-survival autophagy*, Durham theses, Durham University. Available at Durham E-Theses Online: http://etheses.dur.ac.uk/15406/

Use policy

The full-text may be used and/or reproduced, and given to third parties in any format or medium, without prior permission or charge, for personal research or study, educational, or not-for-profit purposes provided that:

- a full bibliographic reference is made to the original source
- a link is made to the metadata record in Durham E-Theses
- the full-text is not changed in any way

The full-text must not be sold in any format or medium without the formal permission of the copyright holders.

Please consult the full Durham E-Theses policy for further details.

Academic Support Office, The Palatine Centre, Durham University, Stockton Road, Durham, DH1 3LE
e-mail: e-theses.admin@durham.ac.uk Tel: +44 0191 334 6107
http://etheses.dur.ac.uk

Investigating a potential oncogenic role for AGR2 in pro-survival autophagy

Lucy Dan

Abstract: Members of the Protein Disulphide Isomerase (PDI) family have essential roles in mediating the oxidation, reduction and isomerisation of disulphide bonds during protein maturation in the endoplasmic reticulum. PDI family members are characterised by the presence of a thioredoxin motif (CXXC) with dual cysteines that permit proteins their oxidoreductase activity. However, PDI proteins that harbour evolutionary divergent thioredoxin motifs have also been identified; the Anterior Gradient-2 (AGR2) protein that possesses a single cysteine residue in its thioredoxin-like domain (CPHS) is one such protein. AGR2 is known to be required for the correct folding and secretion of mucins, the primary gel-forming proteins within mucus. Although its expression is normally restricted to certain secretory and reproductive organs, AGR2 is found derepressed in various cancers. We have previously shown that AGR2 forms a disulphide-dependent interaction with the autophagy receptor Sequestosome 1 (SQSTM1). The oxidation of SQSTM1 is required for the stimulation of autophagy to promote cell survival under conditions of oxidative and proteotoxic stress. The disulphide-dependent interaction between AGR2 and SQSTM1 links AGR2 to autophagy for the first time. Tumours are exposed to high levels of oxidative stress, and thus autophagy can prevent cytotoxicity by removing the cellular components damaged by oxidative stress that may otherwise be toxic to the cell. It is plausible, therefore, that the upregulation of SQSTM1 and AGR2 in human cancers could be involved in the induction of pro-survival autophagy.

Investigating a potential oncogenic role for AGR2 in pro-survival autophagy

Lucy Dan

Thesis submitted for the degree of Masters by Research

Durham University

Department of Biosciences

2023

Contents

Figures and Tables

1. Introduction

3. Results

Abbreviations

ABC – ATP-binding cassette

AGR2 - Anterior gradient-2

AGR3 - Anterior gradient-3

AMPK - Adenosine monophosphate-activated protein kinas

APS - Ammonium persulphate

ATP - Adenosine triphosphate

BCA - Bicinchoninic acid assay

BSA - Bovine Serum Albumin

CC_{50} - 50% cytotoxic concentration

CO_2 - Carbon dioxide

CQ – Chloroquine

C-region – C-terminal region

CRISPR - Clustered Regularly Interspaced Short Palindromic Repeats

C-terminus – Carboxyl-terminus

DAPI - 4',6-diamino-2-phenylindole

dH_2O - De-ionised water

DNA - Deoxyribonucleic acid

DTT – Dithiothreitol

eAGR2 - extracellular AGR2

EBSS - Earle's Balanced Salt Solution

ECACC - European Collection of Authenticated Cell Cultures

ECL - Enhanced chemiluminescence

ER - Endoplasmic reticulum

ERO1 - Endoplasmic reticulum oxidoreductin 1

ERp29 - Endoplasmic reticulum resident protein 29

ERp44 - Endoplasmic reticulum resident protein 44

Fe^{2+} - Ferrous iron

FGF2 - Fibroblast growth factor 2

g - gram

GAMPO - Goat anti-mouse peroxidase

GAPDH - Glyceraldehyde 3-phosphate dehydrogenase

GM130 - Golgi matrix protein 130 kD

GPI - Glycosylphosphatidylinositol

h - hour

HCl - Hydrochloric acid

H_2O_2 - Hydrogen peroxide

H-region – hydrophobic region

iAGR2 - intracellular AGR2

ICGC - International Cancer Genome Consortium

IgG - Immunoglobulin

IP - immunoprecipitation

KCl - Potassium chloride

kDa - kilodaltons

LC3 - Microtubule-associated protein light chain 3

LSM - Laser scanning microscope

LAMP1 - Lysosome-associated membrane glycoprotein 1

mAb - monoclonal antibody

MAPK - mitogen-activated protein kinase

Min – minute

mTOR - Mammalian target of rapamycin

MUC1 - Mucin 1

MUC2 - Mucin 2

MUC5AC - Mucin 5AC

NEM - N-Ethylmaleimide

NMR - Nuclear magnetic resonance

N-region – N-terminal region

N-terminus – amino-terminus

P – P-value

PBS - Phosphate-buffered saline

PDI - Protein disulphide isomerase

PFA - Paraformaldehyde

PI3K - phosphatidylinositol 3-kinase

PrediSi - Prediction of Signal peptides

PVDF - Polyvinylidene difluoride

P4HB - Prolyl 4-hydroxylase, beta polypeptide

ROS – Reactive oxygen species

RPMI - Rosewell Park Memorial Institute medium

RT - Room temperature

SARPO - Swine anti-rabbit peroxidase

SD - Standard deviation

SDS - Sodium dodecyl sulphate

SDS-PAGE - Sodium dodecyl sulphate polyacrylamide gel electrophoresis

SQSTM1 - Sequestosome-1

TBS - Tris-buffered saline

TBS-T - Tris Buffered Saline with Tween

TCGA - The Cancer Genome Atlas

TEMED - N,N,N',N'-Tetramethylethylenediamine

VEGF-A - Vascular endothelial growth factor A

XAG-2 - Xenopus Anterior Gradient-2

Statement of Copyright

The copyright of this thesis rests with the author. No quotation from it should be published without the author's prior written consent and information derived from it should be acknowledged.

Acknowledgements

I would like to thank Prof. Adam Benham for excellent supervision and guidance throughout this project. I would also like to thank the members of Lab 8, including Jamie Thomas, Ianthe Doumas-Calder, Olivia Kent, Steven Bell, Abbi Farley, Kleopatra Papa and Thomas Grange. Lastly, I would like to thank Joanne Robson for helpful microscopy advice.

1. Introduction

1.1. AGR2 is an evolutionary divergent member of the PDI family

As the first compartment in the secretory pathway, the endoplasmic reticulum is the site of protein folding and assembly. Once translocated through the endoplasmic reticulum membrane, newly synthesised proteins undergo various maturation stages that include protein folding, disulphide bond formation and post-translational modifications. These steps are carefully monitored to maintain protein homeostasis (proteostasis). Dysregulations at any given stage can lead to alterations in the secretory pathway and ultimately the cellular proteome, representing an important tipping point into a multitude of diseases (Benham, 2019). Protein folding in the endoplasmic reticulum is assisted by several classical chaperone families, including the peptidyl-prolyl isomerases (PPIases), heat shock proteins (HSPs), and protein disulphide isomerases (PDIs), as well as several unique chaperones and folding enzymes. These proteins are crucial players in the endoplasmic reticulum quality control system for the 'proof-reading' of newly synthesised proteins (Adams, Oster and Hebert, 2019).

Members of the PDI family have essential roles as disulphide oxidoreductases or isomerases, meaning that they mediate the making (oxidising), breaking (reducing) and rearranging (isomerizing) of disulphide bonds in various proteins that are known as "clients" (Fig. 1). In proteins, disulphide bond formation occurs between the -SH groups of two cysteine residues and requires the concomitant transfer of electrons to the PDI family member. The endoplasmic reticulum is relatively more oxidising than the cytosol, which promotes disulphide bond formation in the proteins that translocate into the endoplasmic reticulum (Oka and Bulleid, 2013). The tripeptide glutathione serves as an electron donor in redox reactions and is crucial in maintaining the oxidising environment of the endoplasmic reticulum. An equilibrium exists between glutathione in its reduced (GSH) and oxidised (GSSG) states in distinct cellular compartments. Compared with the cytosol, the endoplasmic reticulum has a high ratio of oxidised glutathione (GSSG) to reduced glutathione (GSH). As such, the oxidation of thiol groups (-SH) to form disulphide bonds (S-S) is favoured in the endoplasmic reticulum but not the cytosol. Disulphide bonds play important stabilising roles in many protein structures (both intramolecular and intermolecular) and can also serve as regulatory switches in redox signalling. PDIs are thus indispensable for regulating protein activities and maintaining proteostasis (Benham, 2012).

To date, 21 members of the *PDI* gene family have been identified, differing in their enzymatic function, tissue expression, and size (Galligan and Petersen, 2012). Phylogenetic analysis identified AGR2 and AGR3 and as evolutionary distant members of the PDI family (Persson *et al.,* 2005). Distinguishing features of PDI family members are endoplasmic reticulum localisation and the presence of a thioredoxin motif (CXXC) with dual cysteines that permit proteins their oxidoreductase activity (Koslov *et al.,* 2010). AGR2 is an unusual PDI family member in that it possesses a single cysteine residue in its evolutionary divergent thioredoxin-like domain (CPHS). AGR2 plays a known role in enabling the correct folding and secretion of intestinal mucins (Park *et al.,* 2009). Through its non-canonical CPHS domain, AGR2 forms mixed disulphides with the mucins MUC1, MUC2 and MUC5AC (Park *et al.,* 2009; Schroeder *et al.,* 2012; Norris *et al.,* 2013). However, the mechanism by which AGR2 mediates mucin disulphide bond formation is currently unclear as AGR2 lacks a redox active thioredoxin motif with dual cysteines.

AGR2 has attracted considerable research interest for its role as an oncoprotein and its derepression has been demonstrated across multiple tumour types, including those of the oesophagus (Pohler *et al.,* 2004), lung (Zhu *et al.,* 2007), ovary (Park *et al.,* 2011), prostate (Zhang *et al.,* 2005), breast (Fletcher *et al.,* 2003) and pancreas (Ramachandran *et al.,* 2008). Despite this, the exact mechanisms by which AGR2 functions as an oncoprotein remain a subject of debate. Recent evidence points to a potential role for AGR2 in pro-survival autophagy, a notion that warrants further investigation. Uncovering the relationship AGR2 has with quality control in the endoplasmic reticulum, mucin secretion and autophagy may contribute to elucidating its oncogenic function.

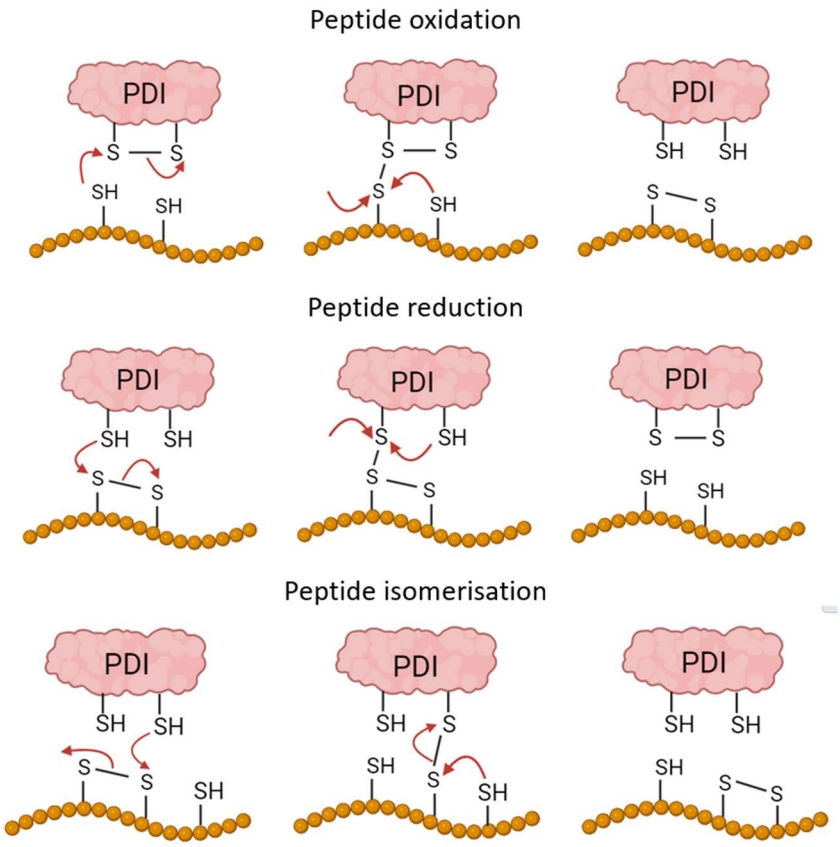

Figure 1. The oxidation, reduction and isomerisation of disulphide bonds in a peptide. Members of the PDI family are characterised by their ability to catalyse such reactions. During redox reactions, peptide oxidation results in PDI reduction and vice versa. The peptide is illustrated in orange. Red arrows indicate direction of electron movement. PDI – protein disulphide isomerase.

1.2. AGR2 structure and biochemical functions

AGR2 possesses many structural features typical of a PDI. The nuclear magnetic resonance (NMR) structure reveals that AGR2 consists of an unstructured N-terminal region followed by a C-terminal thioredoxin-like fold (Fig. 2). The NMR data indicate that the unstructured N terminal region of AGR2 is responsible for its interactions with client proteins (Patel *et al.,* 2013). However, a structural loop from amino acids 131-135 in the thioredoxin-like domain of AGR2 has also been shown to interact sequence-specifically to the peptide sequence TTIYY (Mohtar *et al.,* 2018). It is thus clear that the mechanism by which AGR2 interacts with its client proteins requires further investigation.

AGR2 exists in a monomer-dimer equilibrium. Patel *et al.* 2013 demonstrated that the concentration for AGR2 dimer dissociation is 8.83 μM. Given that the concentration of AGR2 is expected to be higher than this in the endoplasmic reticulum, the authors

concluded that the protein would predominantly be in its dimeric form in this location. The NMR data from Patel *et al.* (2013) demonstrated that intermolecular salt bridges involving E60 and K64 in the C-terminal domain stabilise the dimer. It is plausible that dimerization may enable AGR2 to present multiple binding sites for its client proteins, in particular the multimeric mucin MUC2. It has also been suggested that the dimeric structure of AGR2 may provide a redox capacity equivalent to the canonical thioredoxin motif with dual cysteines (Moidu *et al.,* 2020), but the role of AGR2 dimerization is yet to be proven.

The majority of PDIs harbour a typical KDEL retrieval sequence (Ellgaard and Ruddock, 2005). It is usual for chaperone proteins to remain associated with newly synthesised proteins as they begin to pass through the secretory pathway from the endoplasmic reticulum to the Golgi apparatus (Wu, Newstead and Biggin, 2020). These chaperone proteins must subsequently be retrieved to the endoplasmic reticulum, a process that is mediated by the KDEL receptor. The KDEL receptor is an example of a retrieval sequence as it returns proteins to the compartment they reside in. In contrast, a retention sequence ensures proteins do not leave a specified cellular compartment. The KDEL receptor recognises and binds to the KDEL sequence on resident endoplasmic reticulum proteins present in the Golgi (Miesenböck and Rothman, 1995). The activated KDEL receptor initiates the recruitment of COPI vesicles for retrograde trafficking of chaperone proteins back to the endoplasmic reticulum (Majoul *et al.* 2001). AGR2 exhibits an unconventional KTEL endoplasmic reticulum retrieval sequence (Fig. 2). It has been shown that, in cancer, AGR2 is capable of escaping the endoplasmic reticulum retrieval machinery and can localise to the plasma membrane, extracellular matrix and nucleus (Fourtouna *et al.,* 2009; Gupta, Dong and Lowe, 2012; Fessart *et al.,* 2016). It is tempting to speculate that the non-canonical endoplasmic retrieval motif may lower the affinity of AGR2 to the KDEL receptor, enabling the diverse trafficking of this protein when overexpressed. However, HEK-293T cells transfected with AGR2 mutant constructs in which the KTEL motif was mutated to either a KDEL or a STOP were shown to secrete similar levels of AGR2 to wild-type AGR2 (Fessart *et al.,* 2016). It would thus appear that the extracellular function of AGR2 is independent of the KTEL motif.

Interestingly, it has been reported that dimerization plays a role in AGR2 secretion into the extracellular environment (Maurel *et al.,* 2019). Maurel *et al.* generated monomeric (AGR2 E60A) and dimeric mutant (AGR2 Δ45) proteins in HEK293T cells. It was found that the monomeric mutant displayed a higher secretion rate than wild-type AGR2.

Furthermore, the dimeric mutant was retained intracellularly, suggesting that dimerization may regulate AGR2 secretion. Whether post-translational modifications could also influence the dimerization and secretion of AGR2 is not known. Most secretory proteins become either N-glycosylated or O-glycosylated by a process initiated in the endoplasmic reticulum (Klis *et al.,* 1998; Bennett *et al.,* 2012). Clarke, Rudland and Barraclough (2015) demonstrated that AGR2 is O-glycosylated upon secretion from human and rat cell lines, although it remains to be determined how O-linked glycosylation may alter the biological activities of AGR2.

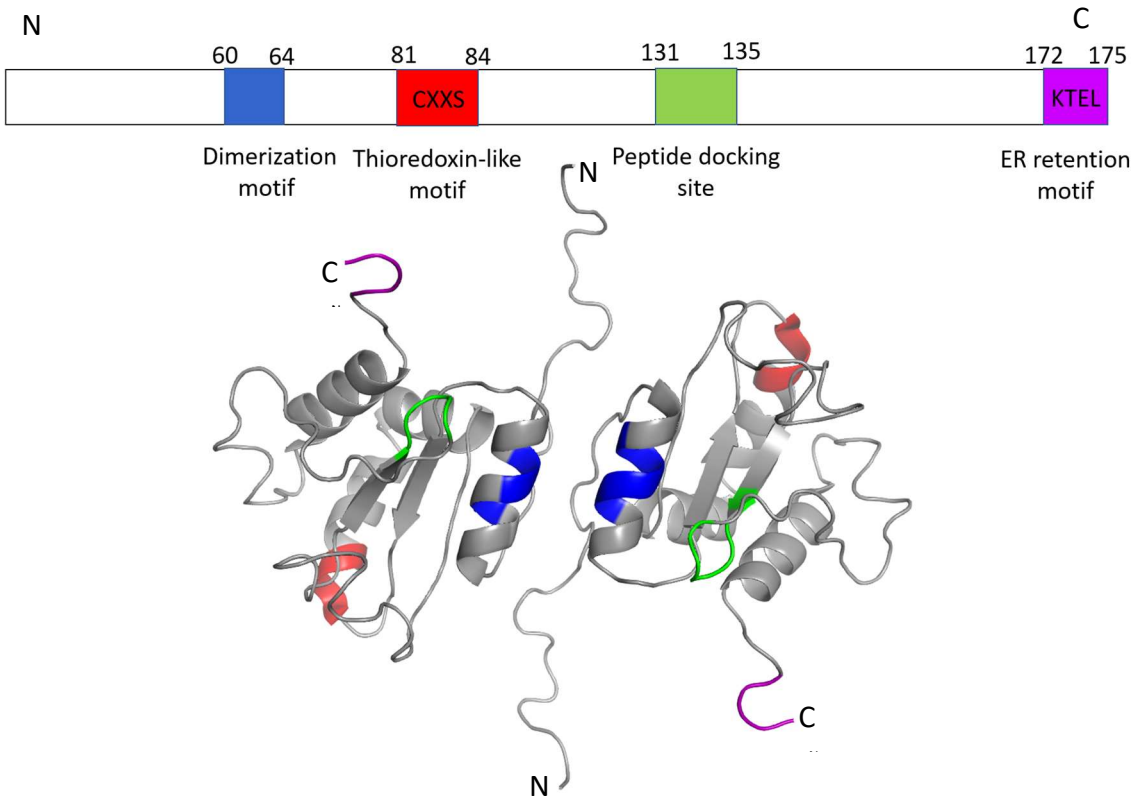

Figure 2. Dimeric AGR2 structure. The schematic panel above represents the full length AGR2 protein. Functional motifs are colour coded with the dimerization motif in blue; the thioredoxin-like motif (CXXS) in red; the peptide docking site in green; and the ER retrieval motif (KTEL) in purple. The solution structure of dimeric AGR2, represented as a cartoon, is shown below. PDBe-KB: O95994. Image generation and analysis conducted in PyMol. N – N-terminus; C – C-terminus.

1.3. The role of AGR2 in maintaining normal intestinal function and in cancer

AGR2 expression is normally restricted to endocrine organs and/or mucus secreting cells, such as the small intestine, colon, stomach, prostate and lungs (Brytova, Vojtesek and Hrstka, 2011). Accordingly, AGR2 is required in healthy cells for the maturation and secretion of mucins (Park *et al.,* 2009), the cysteine-rich glycoproteins that provide mucus

with its viscosity (Fig. 3). Through its thioredoxin-like domain, intracellular AGR2 forms mixed disulphides with the mucins MUC1, MUC2 and MUC5AC (Park *et al.,* 2009; Schroeder *et al.,* 2012; Norris *et al.,* 2013). The importance of AGR2 for the maintenance of intestinal function was demonstrated in an AGR2-deficient mouse, in which the animals are highly susceptible to severe colitis due to their reduced intestinal mucus production (Park *et al.,* 2009). Furthermore, Zheng *et al.* (2005) identified *Agr2* as an important gene in inflammatory bowel disease. Across 2,540 patients with intestinal bowel disease, two single nucleotide polymorphisms (SNPs) in the 5' promoter region of the *Agr2* gene showed significant association with the disease. Moreover, AGR2 was downregulated in patients with the disease compared to healthy controls, supporting the notion that AGR2 is crucial for maintaining intestinal barrier function. It has also been shown that *Agr2* expression is upregulated in the mammary gland during late pregnancy and lactation in normal, healthy mice, presumably to allow for the increased processing and production of milk proteins (Verma *et al.,* 2012). Indeed, Verma *et al.* generated $Agr2^{-/-}$ pregnant mice and found that these animals exhibited a reduced expression of milk proteins during late pregnancy and lactation. Collectively, these findings suggest that AGR2 can mediate the correct folding of client proteins via the PDI activity and controls protein secretion from cells.

AGR2 was first shown to be coexpressed with oestrogen receptor in five breast carcinoma cell lines (Thompson and Weigel, 1998), and it has subsequently been shown that AGR2 is transcriptionally activated by oestrogen (Hrstka *et al.,* 2010). The derepression of AGR2 has since been identified in a multitude of different cancers, including oesophageal (Pohler *et al.,* 2004; O'neill et al, 2017), pancreatic (Ramachandran *et al.,* 2008), ovarian (Park *et al.,* 2011), lung (Zhu *et al.,* 2007), prostate (Zhang *et al.,* 2005), gastric (Tsuji *et al.,* 2015), and head and neck (Ma *et al.,* 2015). Increased levels of AGR2 in prostate and breast cancer has been associated with markedly reduced patient survival (Barraclough *et al.,* 2009; Zhang *et al.,* 2007). Furthermore, a recent meta-analysis evaluating 20 studies containing 3,285 patients revealed that the overexpression of AGR2 predicted poor overall survival and time to tumour progression in all solid tumours (Tian *et al.,* 2017). As a result, AGR2 has attracted recent interest as a potential broad-spectrum drug target. Despite such findings, however, the role of AGR2 in cancer remains incompletely understood. Figure 3 outlines the various pro-oncogenic features of AGR2 that have been proposed thus far.

It is conceivable that the upregulation of AGR2 in cancerous cells allows for the increased secretory demands and levels of protein production that occur during cancer development.

High expression of mutated proteins, a characteristic of cancer cells, can induce folding demands in the endoplasmic reticulum during a response known as ER stress. In turn, ER stress can activate the unfolded protein response (UPR) signalling network, a stress response that serves to reduce the unfolded or misfolded protein load. The UPR achieves this by downregulating the transcription of genes encoding secretory proteins as well as upregulating the expression of genes encoding chaperone proteins (Schröder and Kaufman, 2005). The UPR may be induced chemically by the reducing agent Dithiothreitol (DTT) to prevent disulphide bond formation or by tunicamycin to inhibit glycosylation (Braakman *et al.,* 1992; Wu *et al.,* 2018). Chemically-induced ER stress by tunicamycin and DTT was shown to increase AGR2 expression in both HeLa cervical cancer cell lines and Hep-G2 liver cancer cell lines (Higa *et al.,* 2011). It therefore appears that AGR2 may be important for maintaining homeostasis in the endoplasmic reticulum.

Three signalling pathways, IRE1, PERK and ATF6, play important roles in the activation of the UPR and the maintenance of proteostasis (Schröder and Kaufman, 2005). It is thought that AGR2 expression could be induced by the IRE1α and ATF6 arms of the unfolded protein response because both IRE1α and ATF6α silencing in HepG2 cells resulted in decreased basal *Agr2* mRNA expression and prevented *Agr2* induction upon tunicamycin treatment (Higa *et al.,* 2011). In an analogous fashion, AGR2 silencing in two pancreatic cancer cell lines (FA6 and CFPAC1) resulted in the overexpression of the endoplasmic reticulum stress marker XBP1s (Dumartin *et al.,* 2016). Overall, these findings suggest that a pro-oncogenic role may exist for AGR2 in maintaining proteostasis during ER stress.

AGR2 has also been shown to play an oncogenic role in Barrett's oesophagus, a premalignant condition characterised by increasing levels of oesophageal metaplasia. There is a strong selection pressure for mutating the tumour suppressor p53 in the progression of Barret's metaplasia to adenocarcinoma. A proteomics screen aimed at analysing proteins upregulated in Barrett's oesophagus could therefore be used by Pohler *et al.* (2004) to identify novel p53 regulatory factors. Using this proteomics approach, Pohler *et al.* identified AGR2 as a protein that is universally upregulated in Barrett's oesophagus and functions as an inhibitor of p53. The p53 protein is a stress-activated transcription factor that is considered to be one of the most important classical type tumour suppressors, given that approximately half of human cancers harbour loss of function mutations in the *p53* gene (Marei *et al.,* 2021). Various cell stressors, including DNA damage, are capable of stimulating p53-induced cell cycle arrest and subsequent DNA

repair, or apoptosis. It is now known that AGR2 inhibits p53 activity by the upregulation of Dual Specificity Phosphatase 10, which leads to the inhibition of p38 mitogen-activated protein kinase activity and in turn prevents the phosphorylation and activation of p53 (Hrstka *et al.,* 2016). Successful chemotherapy treatment is reliant upon the induction of DNA damage and the subsequent p53-induced cellular response, directly involving AGR2 with chemotherapy resistance and highlighting this pathway as a promising therapeutic avenue.

Emerging evidence indicates that AGR2 also exerts pro-oncogenic functions as an extracellular protein in the tumour microenvironment (Fig. 3). In a pancreatic ductal adenocarcinoma cell line, the extracellular addition of recombinant AGR2 increased cellular proliferation, migration and invasion (Arumugam *et al.,* 2015). These functions require the involvement of cell surface receptors and Arumugam *et al.* demonstrated that the orphan GPI-linked receptor C4.4A, previously reported as a regulator of metastasis, co-immunoprecipitated with AGR2. Antibodies against AGR2 and/or C.4.4A significantly reduced tumour growth and metastasis, leading to regression of xenograft tumours and improved survival in mouse models (Arumugam *et al.,* 2015). In addition, extracellular AGR2 has been shown to interact with the pro-angiogenic VEGFA and FGF2 (Vascular Endothelial Growth Factor A and Fibroblast Growth Factor 2), enhancing their homodimerization and thereby promoting their pro-angiogenesis activities (Guo *et al.,* 2017). Guo *et al.* further demonstrated that blocking AGR2 activity with a monoclonal antibody reduces angiogenesis and inhibits tumour growth in xenograft models of ovarian cancer.

The presence of AGR2 in the extracellular environment has also been coupled with the acquisition of a pro-inflammatory phenotype. Pancreatic stellate cells are known to be critical for the development of pancreatic ductal adenocarcinoma during a process that is driven by immune activation and inflammation (Sherman *et al.,* 2014). In the PS1 pancreatic stellate cell line, ER stress induced by tunicamycin treatment led to a significant increase in AGR2 expression and significantly increased levels of pro-inflammatory markers (Dumartin *et al.,* 2017). Normal human pancreatic cells treated with the conditioned media from the ER-stressed PS1 cells also became ER-stressed and experienced a significant induction of AGR2 expression. To investigate the link between AGR2 and inflammation, Maurel *et al.* (2019) exposed peripheral blood mononuclear cells from three healthy human volunteers to media conditioned by cells overexpressing AGR2. When present in the extracellular milieu, AGR2 was found to play a direct role in

the chemoattraction of monocytes from peripheral blood mononuclear cells. Monocyte migration was impeded by AGR2 blocking antibodies. These findings revealed a new function for extracellular AGR2 as a pro-inflammatory chemokine.

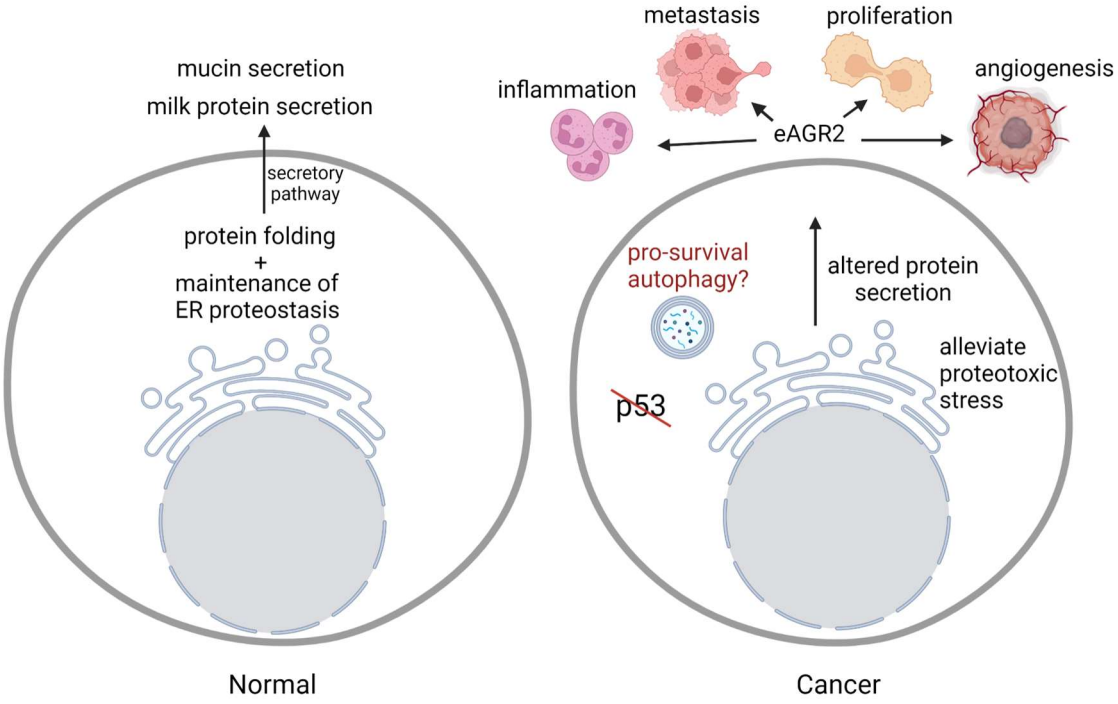

Figure 3. Proposed functions of AGR2 in normal and cancerous cells. The normal cell depicted represents those that are mucus-secreting or have endocrine functions and express AGR2. The cancerous cell shown illustrates one in which AGR2 is derepressed. iAGR2 - intracellular AGR2; eAGR2 - extracellular AGR2. Figure generated in BioRender.

1.4. The potential oncogenic role of AGR2 in pro-survival autophagy

Autophagy is an important mechanism by which cells can degrade dysfunctional or unnecessary cellular components. As a result, autophagy plays a housekeeping role in ensuring that the cellular components that have reached the end of their lifetime are removed. Furthermore, autophagy can serve to eliminate intracellular pathogens and also provide an alternative source of energy to nutrient-stressed cells (Glick, Barth, and Macleod, 2010). Three defined types of autophagy have been determined: macroautophagy, microautophagy, and chaperone-mediated autophagy. In macroautophagy, double membrane vesicles known as autophagosomes form that capture cellular components. The autophagosomes subsequently fuse with an available lysosome to degrade and recycle their contents. In contrast, microautophagy involves the direct

uptake of the dysfunctional or unnecessary cellular components by the lysosome through a process of membrane invagination. In chaperone-mediated autophagy, chaperone proteins deliver a select group of soluble proteins that harbour a specific pentapeptide motif to the lysosome for degradation (Dice, 1990).

In cancer, autophagy can play multifaceted functions in tumour initiation and progression. Indeed, autophagy is essential for protecting cancerous cells from oxidative stress (Taucher *et al.,* 2022); for fulfilling the high metabolic demands of tumours (Pavlides *et al.,* 2012); for contributing to the maintenance of cancer stem cells (Peng *et al.,* 2017); and for mediating cancer drug resistance (Hao *et al.,* 2019). Therefore, the modulation of autophagy is a promising therapeutic strategy in anticancer therapy (Yun and Lee, 2018).

An accumulating body of evidence suggests that oxidative stress regulates the autophagy pathway (McClung *et al.,* 2010; Nezis and Stenmark, 2012; Filomeni, Zio and Cecconi, 2014). Autophagy is a particularly important mechanism for the degradation of proteins and organelles that have been damaged by oxidative stress and may be toxic to the cell. Tumours are exposed to high levels of oxidative stress, and thus autophagy can prevent cytotoxicity in cancer environments (Taucher *et al.,* 2022). Various mechanisms to enable the upregulation of the autophagy pathway in response to oxidative stress have been suggested but the exact process by which the cellular components damaged by reactive oxygen species are targeted to autophagosomes remains undetermined. Evidence presented herein suggests that AGR2, alongside the autophagy receptor protein sequestosome-1 (SQSTM1), may be involved in the induction of autophagy to maintain cellular homeostasis under conditions of oxidative stress.

SQSTM1, also known as the ubiquitin-binding protein p62, is a cysteine-rich protein that delivers ubiquitinated cargos to the autophagosome (Pankiv *et al.,* 2007). Two oxidation-sensitive cysteine residues (C105 and C113) have recently been identified in SQSTM1 (Carroll *et al.,* 2018). Carroll *et al.* further demonstrated that the wild type but not a C105A,C113A-mutant of SQSTM1 was able to stimulate autophagy in mouse embryonic fibroblasts. Autophagy stimulation in the fibroblasts ectopically expressing SQSTM1 increased upon exposure to hydrogen peroxide, suggesting that SQSTM1 plays a functional role in the induction of oxidative stress-induced autophagy. The same study demonstrated that mouse embryonic fibroblasts lacking SQSTM1 or expressing the C105A,C113A mutant were more susceptible to cell death when exposed to oxidative stress than those cells expressing wild type SQSTM1. Moreover, treatment with the autophagy inhibitor chloroquine cancelled out this difference in cell survival between the

cells expressing wild type SQSTM1 and those lacking SQSTM1 or expressing the C105A,C113A mutant, highlighting autophagy as the pro-survival mechanism. These data imply that SQSTM1 oxidation may serve as a regulatory mechanism that evolved to enable the activation of autophagy under conditions of oxidative stress to promote cellular survival. This mechanism could be vital in providing a survival advantage to longer-lived species by offsetting age-related oxidative stress within differentiated cells, such as neurons. It is also plausible that such a mechanism would be upregulated by cancerous cells to enable their survival under oxidative stress conditions. Importantly, cancerous cells experience high levels of oxidative stress as a result of increased metabolism, poor vascular irrigation and gene mutations (Perillo *et al.,* 2020; Arfin *et al.,* 2021).

A recent study investigating the behaviour of AGR2 in the OE19 oesophageal adenocarcinoma cell line adopted an alkylation trapping and immunoprecipitation approach to analyse the AGR2 interactome under oxidising and normoxic conditions (Worfolk *et al.,* 2018). The study demonstrated that an interaction occurs between AGR2 and SQSTM1 that is mediated by disulphide bonds, suggesting AGR2 may potentially play a role in the oxidation of SQSTM1 to induce autophagy. Using SDS-PAGE and Western blotting, Worfolk *et al.* further demonstrated that AGR2 forms a range of complexes that are dispersed upon addition of the reducing agent DTT, supporting the notion that oxidising conditions promote the recruitment of client proteins to AGR2. Given that AGR2 lacks a fully functional CXXC motif, the direct oxidation of SQSTM1 by AGR2 is unlikely. However, as AGR2 is known to form mixed disulphides with its mucin clients (Park *et al.,* 2009), it is plausible that additional oxidation enzymes may assist AGR2 to complete full redox reactions. It is also conceivable that AGR2 could play a chaperone role to assist SQSTM1 into an appropriate conformation for the oxidation of C105 and C113. Alternatively, the dimeric structure of AGR2 may provide the full redox capacity to permit disulphide bond formation between C105 and C113 in SQSTM1.

Analogously to AGR2, SQSTM1 is also upregulated in human cancers, including oesophageal (Adams *et al.,* 2016), breast (Thompson *et al.,* 2003), pancreatic (Mohamed *et al.,* 2015), ovarian (Ju *et al.,* 2016), prostate (Kitamura *et al.,* 2006), and many others. Therefore, it is plausible that the upregulation of AGR2 and SQSTM1 in cancer could be involved in stimulating autophagy to promote cellular survival under conditions of oxidative stress (Fig. 4).

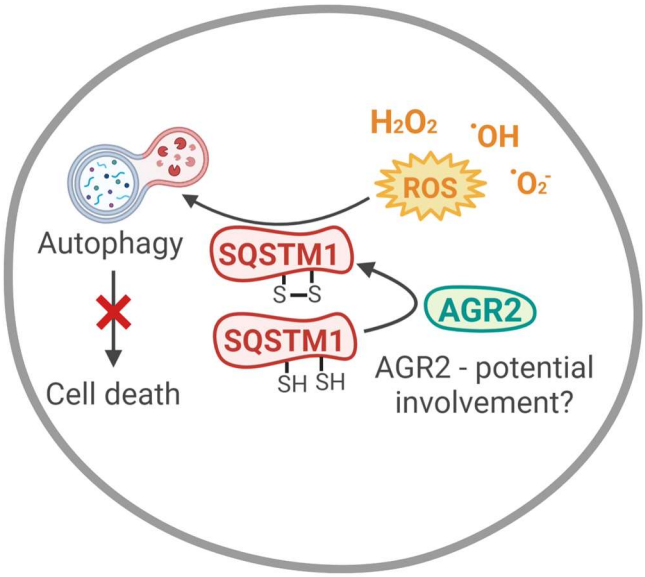

Figure 4. The potential oncogenic roles of SQSTM1 and AGR2 in autophagy to promote cellular survival under conditions of oxidative stress. The oxidation of SQSTM1 is known to be essential for the promotion of autophagy as a pro-survival mechanism under oxidative stress conditions. Oxidative stress occurs when there is an excess of reactive oxygen species (ROS) that can be damaging to proteins, lipids and DNA. Cancer cells are characterised by experiencing high levels of oxidative stress. An interaction occurs between AGR2 and SQSTM1 that is mediated by disulphide (S-S) bonds, suggesting AGR2 may potentially play a role in the oxidation of SQSTM1 to induce pro-survival autophagy.

1.5. The interaction between AGR2 and SQSTM1 poses a topological issue

A topological issue exists as to how AGR2 and SQSTM1 interact. AGR2 normally resides in the endoplasmic reticulum, but can also be localised to the plasma membrane, extracellular matrix and nucleus in the cancer context (Fourtouna *et al.,* 2009; Gupta, Dong and Lowe, 2012; Fessart *et al.,* 2016). In contrast, SQSTM1 is primarily located in the cytosol within the autophagosomes and lysosomes (Berkamp, Mostafavi and Sachse, 2020).

It is possible that AGR2 and SQSTM1 interact at the mucin granule. During the first stage of mucin processing, AGR2 is known to be involved in the folding and polymerisation of mucins in the endoplasmic reticulum (Park *et al.,* 2009). Polymeric mucins are then transported from the endoplasmic reticulum to the Golgi via a mechanism that is poorly understood, but is thought to involve modulated COP-II vesicles to transport the large polymeric mucins (Adler, Tuvim and Dickey, 2013). In the Golgi, mucins undergo further polymerisation as well as O-glycosylation (Kesimer *et al.,* 2010; Bennett *et al.,* 2012). Polymeric mucins are subsequently exported from the trans-Golgi and the post-Golgi

vesicles undergo lateral fusion to form the mature mucin secretory granules (Adler, Tuvim and Dickey, 2013). The exocytosis of these large mucin secretory granules (~1 μm) is highly regulated to ensure mucins are secreted from cells at the appropriate rate (Davis and Dickey, 2008). Recent research showed that the autophagy pathway plays a role in removing excess non-secreted intracellular mucin granules during the resolution of a state of airway inflammation termed mucous metaplasia (Sweeter *et al.,* 2021). In mucous metaplasia, inflammatory signalling leads to an increased expression of mucin genes and an overproduction of mucus (Curran and Cohn, 2010). Mucous metaplasia is characterised by enlarged secretory cells and is persistent in chronic airway diseases such as asthma, chronic obstructive pulmonary disease and cystic fibrosis (Kim *et al.,* 2008; Adler, Tuvim and Dickey, 2013).

It is interesting to speculate whether autophagy may play a similar role in the removal of intracellular mucins in oesophageal cancer or the premalignant condition Barrett's oesophagus. It is conceivable that, in oesophageal adenocarcinoma, SQSTM1 could interact with AGR2 during the autophagic removal of mucins in COP-II vesicles, post-Golgi vesicles or mucin granules. For such a mechanism to occur, AGR2 must remain associated with mucins following their export from the endoplasmic reticulum. This is entirely possible, given that AGR2 is known to escape the endoplasmic reticulum retrieval machinery in cancerous cells (Fessart *et al.,* 2016; Guo *et al.,* 2017; Dumartin *et al.,* 2017).

Because AGR2 can be secreted from cancer cells (Tsuji *et al.,* 2015, Guo *et al.,* 2017), it is also plausible that AGR2 may follow the secretory pathway and be exocytosed, before being endocytosed back into the cell to be degraded by selective autophagy mediated by SQSTM1. Such a mechanism would similarly enable AGR2 and SQSTM1 to be in proximity for their interaction. Appropriately, AGR2 contains a motif characteristic of the secretory signal-peptide, which suggests that AGR2 may be able to follow the classical secretory pathway along the ER-Golgi-plasma membrane route (Gupta, Dong and Lowe, 2012).

The interaction between AGR2 and SQSTM1 has thus far only been identified in oesophageal adenocarcinoma (Worfolk *et al.,* 2019), and therefore is perhaps as a result of perturbed oncogenic signalling. However, further work is required to establish whether AGR2 interacts with SQSTM1 in non-malignant cells. Overall, it is clear that the topological issue regarding the AGR2-SQSTM1 interaction requires further investigation, particularly regarding the potential involvement of mucin granule synthesis and autophagy in this interaction.

1.6. Therapeutic strategies and future outlooks

Autophagy has been demonstrated to play multifaceted functions in the initiation and progression of cancer, and thus is a promising therapeutic strategy in anticancer therapy. Indeed, clinically-approved autophagy inhibitors, such as chloroquine, have been successfully used in combination with other agents for the treatment of various tumour types (Chude and Amaravadi, 2017). Chloroquine inhibits autophagy by preventing autophagosome-lysosome fusion (Mauthe *et al.,* 2018). SQSTM1 has also shown promising results as a drug target in cancer. PTX80 is a novel inhibitor of SQSTM1 that induces proteotoxic stress and in turn activates the unfolded protein response, resulting in apoptosis (Kalid *et al.,* 2022). Kalid *et al.* reported significant inhibition of tumour growth in mice bearing various cell line xenografts compared to vehicle control and the treatment was well tolerated. The overexpression of AGR2 and its multitude of reported oncogenic functions have also made it an attractive therapeutic target. Guo *et al.* (2016) generated a humanized antibody 18A4 that targets AGR2. The study demonstrated that 18A4 treatment in a subcutaneous ovarian cancer xenograft tumour model reduced tumour volumes by more than 50% compared with the vehicle control group without any reported side effects. Another intriguing therapeutic avenue could involve targeting the AGR2-SQSTM1 interaction with antioxidants, as oxidising conditions have been shown to induce the formation of AGR2 complexes (Worfolk *et al.,* 2019).

AGR2 has attracted considerable research interest for its role as an oncoprotein, although the exact mechanisms by which it functions remain a subject of debate. The present thesis investigates the role of AGR2 in oesophageal adenocarcinoma to further investigate the intriguing interaction that was discovered with SQSTM1 in this tumour type (Worfolk *et al.,* 2019). Using reducing and non-reducing SDS-PAGE and subsequent Western blotting, the presence of disulphide-dependent AGR2 complexes in oesophageal adenocarcinoma cell lines will be investigated. The AGR2-SQSTM1 interaction will also be verified through immunoprecipitation experiments in oesophageal adenocarcinoma cell lines. Immunofluorescence experiments will be utilised to analyse the cellular localisation of AGR2 and SQSTM1, and explore the topological conundrum as to how these two proteins interact. Use of SDS-PAGE and Western blotting will also permit investigation into any potential alteration to the levels of AGR2 in oesophageal adenocarcinoma cell lines following autophagy stimulation via cell stress treatments. The secretion of AGR2 from oesophageal adenocarcinoma cells will also be explored by subjecting culture media to SDS-PAGE and Western blotting with an AGR2 mAb. AGR2

appears to be at the centre of a complex relationship between endoplasmic reticulum quality control, mucin secretion, autophagy and cancer; uncovering the connection between AGR2 and the aforementioned functions may provide a holistic understanding of its oncogenic role.

2. Materials and Methods

2.1. Antibodies and chemicals

The rabbit monoclonal anti-AGR2 (D9V2F) was purchased from Cell Signalling Technologies. The mouse monoclonal anti-p62,SQSTM1 (66184-1-Ig), mouse monoclonal anti-LC3 (66139-1-Ig) and mouse monoclonal anti-GAPDH (60004-1-Ig) were purchased from Proteintech. The rabbit monoclonal anti-AGR2 (ab76473) and mouse monoclonal anti-β-actin (ab8224) were purchased from Abcam. The mouse monoclonal anti-GM130 (610823) was purchased from BD Biosciences. The mouse monoclonal anti-PDI,P4HB RL90 (MA3-019) was purchased from Thermo Fisher Scientific. Secondary antibodies used for immunofluorescence experiments were donkey anti-rabbit Alexa Fluor 488 (A21206) and goat anti-mouse Alexa Fluor 633 (A21136) from Thermo Fisher Scientific. Goat anti-mouse HRP (GAMPO - P0447) and swine anti-rabbit HRP (SARPO - P0217) from Agilent were used as secondary antibodies for Western blotting experiments.

For immunofluorescence experiments, the dilutions of the primary antibodies used were: anti-AGR2 (D9V2F), 1:200; anti-AGR2 (ab76473), 1:250; anti-p62,SQSTM1 (66184-1-Ig), 1:250; anti-GM130 (610823), 1:200; anti-PDI,P4HB RL90 (MA3-019), 1:200; anti-LC3 (66139-1-Ig), 1:200. The dilutions for the secondary antibodies used in immunofluorescence experiments were 1:1,000 for both donkey anti-rabbit Alexa Fluor 488 and goat anti-mouse Alexa Fluor 633. The dilutions of the primary antibodies used for Western blotting were: anti-AGR2 (D9V2F), 1:1,000; anti-p62,SQSTM1 (66184-1-Ig), 1:1,000; anti-GAPDH (60004-1-Ig), 1:5,000; anti-AGR2 (ab76473), 1:5,000; anti-β-actin (ab8224), 1:10,000. The dilutions for the secondary antibodies used for Western blotting were 1:3,000 for both GAMPO P0447 and SARPO P0217.

Unless stated otherwise, all chemicals were purchased from Sigma-Aldrich.

2.2. Cell lines and culture

The OE19 (JROECL19), OE21 (JROECL21) and OE33 (JROECL33) cell lines were obtained from ECACC (European Collection of Cell Cultures). The OE19, OE21 and OE33 cell lines were established from a stage III adenocarcinoma of the gastric cardia/oesophageal gastric junction, a stage IIA squamous carcinoma of mid oesophagus, and a stage IIA adenocarcinoma of the lower oesophagus, respectively. Cells were grown in Roswell Park Memorial Institute (RPMI) medium supplemented with 10% fetal bovine serum (Sigma), 1% penicillin/streptomycin (Invitrogen Thermo Fisher), and 2 mM

GlutaMAX (Invitrogen Thermo Fisher). Cells were maintained at 37 °C and a humidified atmosphere of 5% CO_2. Cells were subcultured twice a week at a split ratio of 1:10. Prior to treatment, cells were grown to 70-80% confluence.

2.3. Cell treatments

Urea hydrogen peroxide tablets (Sigma) were dissolved in dH_2O and used fresh prior to treatment. Stock solutions of chloroquine (Sigma) were made up in RPMI media and either frozen at -20 °C prior to treatment or used fresh. Cells were treated with fresh RPMI media supplemented with the required chemical to make up the indicated concentration and returned to a 37 °C incubator for duration of the treatment. For salt stress treatments, cells were incubated in Earle's Balanced Salts Solution (with sodium bicarbonate, without calcium chloride and magnesium sulphate) from Sigma (E6267) at 37 °C for the indicated treatment time. For nutrient starvation, cells were incubated at 37 °C for the indicated treatment time in RPMI media prepared as described previously excluding the fetal bovine serum and GlutaMAX to create a non-glucose, non-glutamine medium. Cells were washed twice with phosphate buffered saline (PBS) from Thermo Fisher Scientific and lysed immediately after treatment.

2.4. Cell lysis

Cells were washed with ice-cold PBS then scraped into MNT lysis buffer (100 mM NaCl, 30 mM Tris, 20mM 4-morpholineethanesulfonic acid, made up to pH 7.4, with the addition of 1% Triton X-100 and the protease inhibitors antipain, chymostatin, pepstatin A and leupeptin at 10 μg mL^{-1} each). Cell lysates were then left on ice for 30 min and subsequently centrifuged at 13,000 rpm for 10 min at 4 °C. The supernatant was collected and used fresh or stored at -20 °C and thawed before use.

2.5. Protein determination

Protein concentration was measured using the Pierce BCA Protein Assay Kit (Thermo Fisher Scientific) using the microplate procedure. Bovine serum albumin (BSA) was diluted with lysis buffer to produce a series of standard protein concentrations ranging from 0-2,000 μg/mL. Standards and lysates (25 μL of each) were pipetted into a 96-Well plate and 200 μL of the BCA working reagent was added to each well. The plate was mixed on a plate shaker in a 37 °C room for 30 min. The plate was allowed to cool to room temperature and the absorbance at 562 nm was measured on a plate reader. A standard curve was generated from the absorbance values of the BSA standards, allowing the protein concentrations of the samples to be estimated.

2.6. SDS-PAGE and Western blotting

Between 20 and 50 µg of total protein per sample were used for SDS-PAGE and Western blotting analysis. Sample proteins were prepared by the addition of 2 X Laemmli sample buffer (2.1% SDS, 26.3% glycerol, 0.01% bromophenol blue, and 65.8 mM Tris-HCl at pH 6.8). Dithiothreitol (DTT) at 10% was added where reducing conditions were used, but was omitted under non-reducing conditions. Lysis buffer was added to ensure an equal volume of sample was loaded into each well of the SDS-PAGE gel. Samples were prepared by boiling at 95 °C for 5 min and then were run on a 12% polyacrylamide gel in a Hoefer™ Mighty Small™ II Mini Vertical Electrophoresis Systems tank (Thermo Fisher Scientific). The resolving gel (0.4 M Tris at pH 8.8, 40% acrylamide, 0.1% ammonium persulphate (APS), 0.1% sodium dodecyl sulfate (SDS), and 0.001% N,N,N',N'-Tetramethylethylenediamine (TEMED)) was cast first and covered with a layer of dH_20. Once set, the water layer was removed and a 10-well gel comb was inserted. The stacking gel (0.125 M Tris at pH 6.8, 6% acrylamide, 0.1% APS, 0.1% SDS, and 0.001% TEMED in dH_20) was then cast and left to polymerise. Gels were run at 20 mA for ~45 min in Tris-Glycine SDS Running Buffer (25 mM Tris, 192 mM Glycine, and 0.1% SDS in dH_20, pH 8.3).

Following separation by SDS-PAGE, proteins were wet-transferred from the gel onto a polyvinylidene fluoride (PVDF) membrane using the Bio-Rad Mini-PROTEAN Tetra electrophoresis system. PDVF membranes were first activated in methanol for 10 seconds. Proteins were transferred onto membranes in transfer buffer (190 mM glycine, 25 mM Tris base, and 20% methanol in dH_2O) at either 150 mA for 2 hours or 30 V overnight. Membranes were then either analysed by Ponceau S staining or were blocked with 5% milk diluted in Tris-Buffered Saline Tween-20 (TBS-T made up of 25 mM Tris base, 136 mM NaCl, 2.7 mM KCl in dH_20, pH 8.0, 0.1% Tween 20) for 45 min at room temperature. After washing five times in TBS-T (5 min each), membranes were incubated with primary antibodies on a plate shaker for 1 hour at room temperature or overnight at 4 °C. Membranes were washed as above and then incubated with secondary antibodies for 1 hour at room temperature. Membranes were washed as above and then incubated for 5 min with the Pierce ECL Western Blotting Solution (Thermo Fisher Scientific) and signals were detected by chemiluminescence on an Invitrogen iBright Imaging System (Themo Fisher Scientific).

2.7. Ponceau S staining

After the transfer stage of Western blotting, PDVF membranes were washed in dH_2O in triplicate (1 min each). Membranes were then incubated in Ponceau S solution (0.1% Ponceau S (w/v) from Sigma-Aldrich diluted in dH_2O, with 5% acetic acid) for 10 min at room temperature on a rocker. Membranes were then rinsed in dH_2O for 30 seconds and subsequently photographed. To remove the stain, membranes were washed once in TBS-T for 5 min then rinsed again in dH_2O for 30 seconds.

2.8. Immunoprecipitation

Cells were lysed using the aforementioned protocol then snap frozen in liquid nitrogen and stored at -20 °C prior to being thawed for immunoprecipitation analysis. Protein A-Sepharose beads (Sigma) were washed twice with lysis buffer and incubated with primary antibodies for 1 hour at 4 °C at a ratio of 15 µl:35 µl (antibody:Protein A-Sepharose beads) with rotational shaking. The antibody bead mixture was washed three times in lysis buffer (5 min each) and subsequently incubated with 250 µL cell lysate overnight at 4°C with rotational shaking. The beads were washed once with lysis buffer, retaining the supernatant. The lysate bead mixture was eluted using 50 µl of 2 X Laemmli sample buffer. Following the addition of 10% DTT, samples were heated to 95 °C for 5 min. Samples were then loaded onto an SDS-PAGE gel and subsequently analysed by Ponceau S and Western blotting. Each sample was loaded alongside remaining lysate that had not been incubated with beads or antibodies as a control.

2.9. Immunofluorescence

OE19 and OE33 cells were seeded on coverslips in 12-well plates. Cells were incubated at 37 °C and 5% CO_2 in RPMI medium until ~60% confluency. After any indicated treatments, cells were washed twice (5 min each) in phosphate buffered saline with magnesium and calcium (PBS++) from Thermo Fisher Scientific. Cells were then fixed in 4% paraformaldehyde (PFA) in PBS++ for 10 min at room temperature. Cells were washed twice in PBS++ (5 min each) and then permeabilised in 0.1% Triton X-100 in PBS++ for 10 min (omitted for non-permeabilised analysis of cells). Cells were washed in triplicate in PBS++ (5 min each) and then blocked in 2% bovine serum albumin (BSA) in PBS++ for 30 min at room temperature. Coverslips were incubated with primary antibodies diluted in PBS++ (concentrations given in section 2.1) for 2 hours at room temperature or overnight at 4 °C in a closed container with wetted Kimwipes to maintain a humid atmosphere. Coverslips were washed in PBS++ in triplicate (5 min each) and then

incubated with the appropriate secondary antibody at a 1:500 dilution in PBS++ for 1 hour at room temperature in a dark, humidified container. Coverslips were washed in PBS++ in triplicate (5 min each) in the dark. Nuclear DNA was stained by incubation with 25 µL of 5 µg/mL 4',6-diamino-2-phenylindole (DAPI) solution for 10 min at room temperature in the dark. Coverslips were washed once in PBS++ for 5 min in the dark. Coverslips were mounted on slides with 5 µL of VECTASHIELD Hardset Antifade Mounting Medium (Vector Laboratories) and left for 15 min to set at room temperature in the dark. Coverslips were then sealed onto microscope slides with nail varnish and left to set. Slides were kept at 4 °C overnight in the dark prior to imaging on a confocal microscope (Zeiss 800) using a 63X Oil objective. Images were analysed using ZEISS ZEN 3.5 (blue edition) and ImageJ software. Where multiple antibodies were used for co-staining, these were applied simultaneously.

2.10. Live cell imaging

OE19 cells were incubated in a glass-bottom culture dish at 37 °C and 5% CO_2 in RPMI medium until ~60% confluency. Cells were then incubated in RPMI medium containing 7 µg/ml CellMask™ Deep Red plasma membrane stain (Thermo Fisher Scientific - C10046) for the indicated treatment time. Cells were washed twice with fresh RPMI (warmed to 37 °C) and then imaged with a Zeiss LSM 880 confocal microscope at X63 magnification. During live cell observation, the microscope was maintained at 37°C and 5% CO_2.

2.11. Cell viability assay

To determine cell viability, the Orangu assay (Cell Guidance Systems Ltd, Cambridge, UK) was used according to the manufactory guidelines. Briefly, 5 x 10^3 OE19 and 5 x 10^3 OE33 cells were seeded in 96-well plates. Cells were treated with increasing concentrations of chloroquine (0, 2, 4, 8, 16, 32, 64, 128, 256 µM) and incubated at 37 °C and 5% CO_2. After 48 hours of incubation, 10 µL of Orangu cell counting solution was added to each well and incubated for 120 min at 37 °C and 5% CO_2. After incubation, absorbance was measured at a wavelength of 450 nm. To calculate percentage cell viability, the absorbance of untreated cells was used as a reference of 100% and the absorbance of chloroquine-treated cell cultures were correlated to them.

2.12. Cell counting

In an Eppendorf tube, 100 µL of cells was mixed with 400 µL 0.4% Trypan Blue Solution (Thermo Fisher Scientific). Trypan Blue cell suspension (100 µL) was applied to the

chambers of a haemocytometer. The number of live cells were counted within each of the gridlines of the haemocytometer using the EVOS Cell Imaging System at 10X magnification. The final estimation of viable cells/mL in the original cell suspension was calculated.

2.13. Statistical analysis

Western blot quantification was performed by densitometry analysis using ImageJ. Intracellular aggregates of SQSTM1, LC3 or AGR2 were counted by eye with the assistance of the cell counter tool in ImageJ. Where unpaired Student's t-tests were carried out, sample data met the requirements for normality as determined by the Shapiro-Wilk and the Jarque-Bera test for skewness and kurtosis. All statistical tests are two-tailed. Sample sizes are given in the relevant figure legends. All statistical tests were implemented in R v4.0.3.

2.14. Signal peptide prediction

The human AGR2 amino acid sequence was taken from UniProt (reference 095994). The PrediSi (Prediction of Signal Peptides) online tool was used for the prediction of signal peptide sequences and signal sequence cleavage positions as described previously (Hiller *et al.,* 2004). The Eukaryotic group was selected for analysis. PrediSi is available at http://www.predisi.de/predisi/index.html.

3. Results

3.1. AGR2 forms disulphide-dependent complexes in OE19 cells

A proteomics screen identified AGR2 as a protein that is universally upregulated in Barrett's oesophagus, a premalignant condition characterised by increasing levels of oesophageal metaplasia (Pohler *et al.,* 2004). Previous work in the laboratory has also demonstrated that AGR2 is expressed in certain oesophageal adenocarcinoma cell lines (Worfolk *et al.,* 2019). To follow up on these findings, the expression of AGR2 in three oesophageal adenocarcinoma cell lines (namely, the OE19, OE21 and OE33 cells) was investigated. The OE19, OE21 and OE33 cell lines were established from a stage III adenocarcinoma of the gastric cardia/oesophageal gastric junction, a stage IIA squamous carcinoma of mid oesophagus, and a stage IIA adenocarcinoma of the lower oesophagus, respectively.

The single cysteine residue of AGR2 has been reported to form mixed disulphide bonds with its client proteins (Park *et al.,* 2009; Schroeder *et al.,* 2012; Norris *et al.,* 2013). Therefore, samples were separated by both reducing and non-reducing SDS-PAGE to identify the presence of disulphide-dependent complexes using Western blotting analysis with the ab76473 AGR2 mAb. Under reducing conditions, DTT was added as the reducing agent to the sample to break any intermolecular or intramolecular disulphide bonds. DTT was omitted under the non-reducing conditions, allowing disulphide bonds to remain intact. Running samples through reducing and non-reducing SDS-PAGE can thereby indicate the presence or absence of disulphide-dependent complexes.

The results of a representative experiment show that AGR2 was strongly expressed in OE19 cells, but was not detectable by Western blotting in OE21 and OE33 cells (Fig. 5). In these OE19 cells, monomeric AGR2 is visible as a distinct band at ~19 kDa. Under non-reducing conditions, the band at ~37 kDa is likely to be homodimeric AGR2 and many higher molecular weight complexes (~50-80 kDa) are also visible. As expected, these AGR2 complexes in the OE19 cell lysates were dispersed by the addition of the reducing agent DTT to the sample buffer, and thus are disulphide dependent (Fig. 5). Therefore, it is clear that endogenous AGR2 can form disulphide-dependent complexes in OE19 cells.

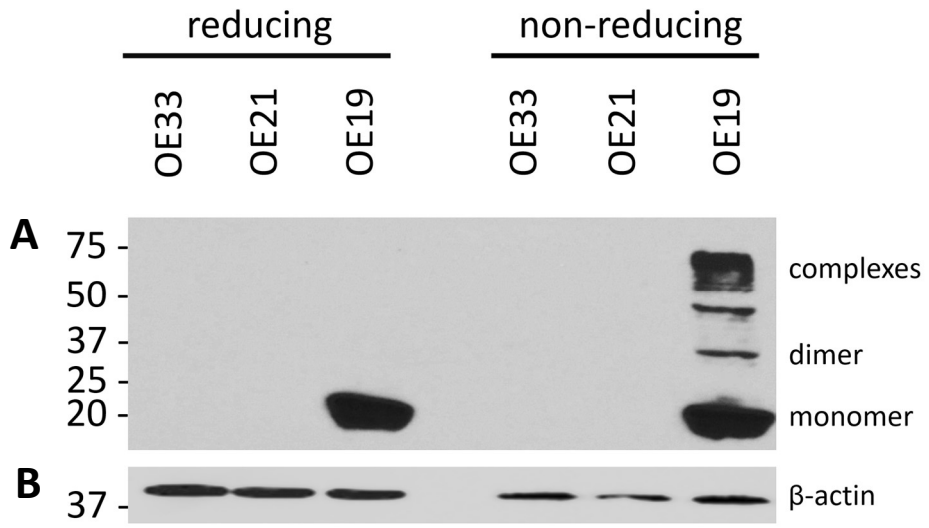

Figure 5. AGR2 expression in oesophageal adenocarcinoma cell lines under reducing and non-reducing conditions. (A) OE19, OE21 and OE33 cells were lysed, analysed by reducing and non-reducing SDS-PAGE and subjected to Western blotting with the ab76473 AGR2 mAb. **(B)** The membrane was stripped and reprobed for β-actin as a Western blot control. kDa markers are displayed on the left.

3.2. AGR2 resides in the endoplasmic reticulum in OE19 cells

Given that high levels of AGR2 expression had been identified in the OE19 cells (Fig. 5), this cell line was used to further investigate the biochemical features and potential oncogenic function of AGR2. The intracellular distribution of AGR2 in OE19 cells was explored using immunofluorescence and confocal microscopy. AGR2 normally resides in the endoplasmic reticulum, but can also be localised to the plasma membrane and nucleus in the cancer context (Fourtouna *et al.,* 2009; Gupta, Dong and Lowe, 2012; Fessart *et al.,* 2016). OE19 cells on coverslips were fixed, permeabilised and stained for AGR2 and the cis-Golgi marker GM130, or AGR2 and the ER marker P4HB (Fig. 6). AGR2 did not colocalize with GM130, as expected. However, the majority of AGR2 did colocalize with P4HB in the endoplasmic reticulum.

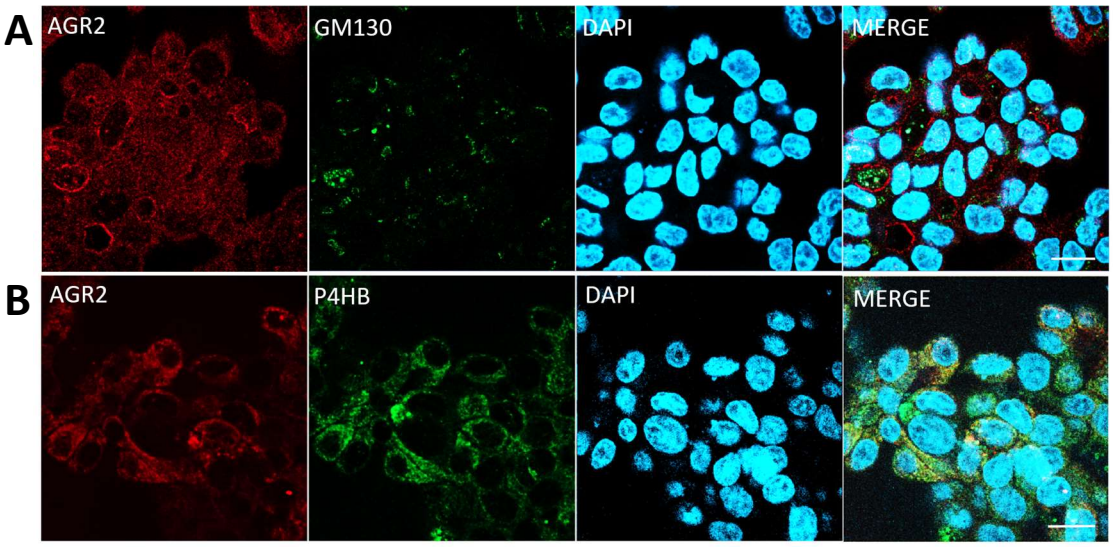

Figure 6. Intracellular distribution of AGR2 in OE19 cells. OE19 cells on coverslips under control conditions were fixed, permeabilised and costained for AGR2 (red) and GM130 (green) **(A)**, or AGR2 (red) and P4HB (green) **(B)**, and subsequently analysed on a Zeiss 800 confocal microscope at X63 magnification. Nuclei are stained for with DAPI. Scale bar: 10 μm.

3.3. AGR2 interacts with SQSTM1 in OE19 cells

Endogenous AGR2 forms disulphide-dependent complexes in OE19 cells (Fig. 5). Proteomics experiments have previously identified an interaction between AGR2 and the autophagy receptor SQSTM1 that is mediated by disulphide bonds (Worfolk *et al.,* 2019). Data produced by Carroll *et al.* (2018) showed that the oxidation of SQSTM1 stimulates autophagy to promote cellular survival under oxidative stress conditions. These findings link AGR2 to a potential role in pro-survival autophagy. To further investigate this notion, the interaction between AGR2 and SQSTM1 required verification in the OE19 cell line. It was previously demonstrated that AGR2 was not detectable by Western blotting in the OE33 cells (Fig. 5), and thus this cell line was used as a negative control. OE19 and OE33 cell lysates were subjected to immunoprecipitation (IP) with the 66184-1-Ig SQSTM1 mAb before analysis by SDS-PAGE and Western blotting with the ab76473 AGR2 mAb. For confirmation, this experiment was also repeated in the reverse such that OE19 and OE33 cell lysates were subjected to IP with the ab76473 AGR2 mAb before analysis by SDS-PAGE and Western blotting with the 66184-1-Ig SQSTM1 mAb.

Bands at ~19 kDa corresponding to AGR2 monomers were visible in the OE19 lysate and OE19 IP SQSTM1 lanes, demonstrating that endogenous AGR2 interacts with SQSTM1 in the OE19 cells (Fig. 7A). As expected, the monomeric AGR2 bands were entirely absent from OE33 lysate and OE33 IP SQSTM1 lanes (Fig. 7A). In addition, bands

corresponding to SQSTM1 at ~60 kDa were present in both the OE19 lysate lane and OE19 IP AGR2 lane, which verifies the interaction between SQSTM1 and AGR2 (Fig. 7B). The SQSTM1 band was also visible in the OE33 lysate lane but absent from the OE33 IP AGR2 lane, as expected due to the absence of AGR2 expression in the OE33 cells (Fig. 7B). GAPDH was probed for as a control to demonstrate the equal loading of cell lysates across wells (Fig. C & D). Staining with ponceau S was used to confirm the presence of equal amounts of immunoglobulin (Ig) in both IPs as a Western blotting control (Fig. 7E & F).

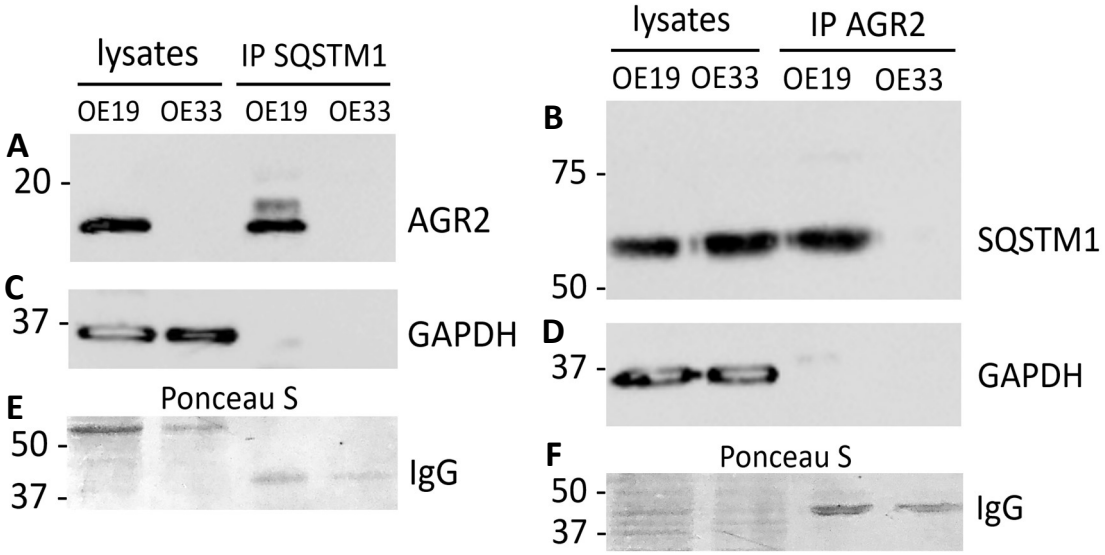

Figure 7. SQSTM1 co-immunoprecipitates with AGR2 in OE19 cells. OE19 and OE33 cell lysates were either analysed by SDS-PAGE and subsequent Western blotting with the ab76473 AGR2 mAb or were subjected to immunoprecipitation (IP) with the 66184-1-Ig SQSTM1 mAb before analysis by SDS-PAGE and Western blotting with the ab76473 AGR2 mAb **(A)**. OE19 and OE33 cell lysates were also analysed by SDS-PAGE and subsequent Western blotting with the 66184-1-Ig SQSTM1 mAb or were subjected to immunoprecipitation (IP) with the ab76473 AGR2 mAb before analysis by SDS-PAGE and Western blotting with the 66184-1-Ig SQSTM1 mAb **(B)**. Membranes were reprobed for GAPDH as a Western blotting control **(C, D)**. Staining with ponceau S was used to confirm the presence of IgG in both IPs as a Western blotting control **(E, F)**. Cells were grown to ~80% confluency to provide sufficient protein concentrations for IP analysis. kDa markers are given on the left. IP – immunoprecipitation; Ig – immunoglobulin.

To further investigate the AGR2-SQSTM1 interaction, the intracellular distribution of these two proteins was explored using immunofluorescence to investigate any potential colocalization between them. SQSTM1 serves to sequester ubiquitylated cytoplasmic components to the nascent autophagic vesicles (Ponpuak *et al.,* 2010). Consequently,

SQSTM1 can be used as a autophagosome marker in immunofluorescence experiments (Carroll *et al.,* 2018). How AGR2 and SQSTM1 interact therefore poses a topological issue, as the majority of AGR2 was found to localize in the endoplasmic reticulum (Fig. 6).

The punctate distribution of SQSTM1 marking the autophagosomes is visible in Figure 8. Although there is not clear colocalization between AGR2 and SQSTM1, some areas of overlap are visible (arrowheads; Fig. 8). It is clear that the mechanism by which AGR2 may be capable of escaping the endoplasmic reticulum retrieval machinery in order to interact with SQSTM1 requires further investigation.

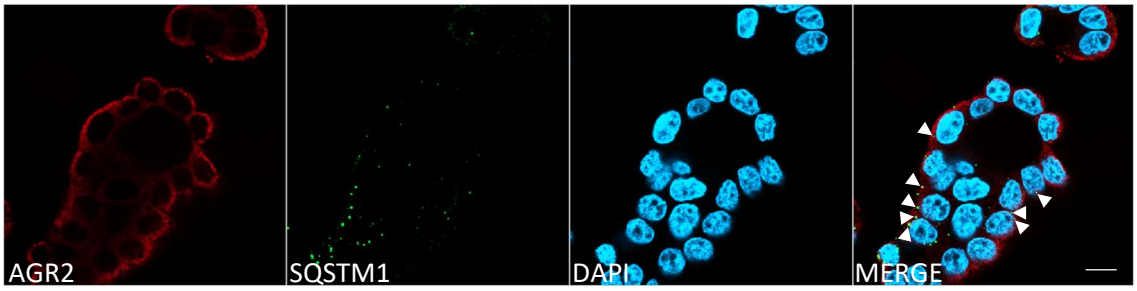

Figure 8. Intracellular distribution of AGR2 and SQSTM1 in OE19 cells. OE19 cells on coverslips under control conditions were fixed, permeabilised and costained for AGR2 (red) and SQSTM1 (green), and subsequently analysed on a Zeiss 800 confocal microscope at X63 magnification. Nuclei are stained for with DAPI. Arrowheads show the SQSTM1-labelled autophagosomes that overlap with AGR2 staining. Scale bar: 10 µm.

3.4. The effect of cell stress treatments on the intracellular distribution and levels of AGR2

The interaction with SQSTM1 links AGR2 to the induction of autophagy in response to oxidative stress conditions for the first time. Therefore, in the following experiments OE19 cells received various treatments known to induce autophagy to investigate the behaviour and function of AGR2 under such conditions. A disbalance in calcium homeostasis can initiate endoplasmic reticulum stress, which in turn promotes the stimulation of autophagy via the unfolded protein response (Taucher *et al.,* 2022). Therefore, cells were incubated in Earle's Balanced Salts Solution (EBSS) that excludes calcium chloride and magnesium sulphate to investigate any potential increase in autophagy stimulation. Production of reactive oxygen species can also lead to a rapid induction of autophagy through proteins that are sensitive to oxidative stress. Such proteins include AMPK, which is activated by H_2O_2 to promote autophagy (Zmijewski *et al.,* 2010), and reduced glutathione that has been shown to stimulate autophagy when oxidised (Desideri, Filomeni, and Ciriolo, 2012). OE19 cells were thus exposed to H_2O_2

treatment to investigate any potential involvement of AGR2 in a pro-survival autophagy response to oxidative stress. A non-glucose, non-glutamine RPMI medium was also used to subject OE19 cells to nutrient starvation, which is known to induce autophagy via signalling through PI3K (phosphatidylinositol 3-kinase)/AMPK (adenosine monophosphate-activated protein kinase) and other nutrient-sensing pathways (Alers *et al.,* 2012; Chiao *et al.,* 2013). Nutrient starvation often leads to metabolic stress and a higher demand for ATP, leading to mitochondrial overburden and electron leakage that ultimately triggers excessive generation of reactive oxygen species (Ophuis *et al.,* 2009; Taucher *et al.,* 2022). Therefore, nutrient deprivation is also thought to trigger autophagy indirectly through the cellular response to oxidative stress (Taucher *et al.,* 2022). Other mechanisms yet to be elucidated may also stimulate autophagy in response to endoplasmic reticulum, oxidative or nutrient stress.

Given the potential involvement of AGR2 in pro-survival autophagy, alongside the topological issue of the AGR2-SQSTM1 interaction, it was considered appropriate to investigate the intracellular distribution of AGR2 during autophagy stimulation. Indeed, it is possible that AGR2 could escape the endoplasmic reticulum retrieval machinery solely during endoplasmic reticulum, oxidative and/or nutrient stress. For instance, pathways involved in unconventional protein secretion (the secretion of proteins via a route bypassing the endoplasmic reticulum and/or Golgi) are stimulated in human cells by stressors such as nutrient starvation and endoplasmic reticulum stress (Gee *et al.,* 2011; Cruz-Garcia *et al.,* 2014). Therefore, OE19 cells on coverslips received 20 min H_2O_2 treatment (3mM); 48 h salt stress treatment (cultured in Earle's Balanced Salts Solution without calcium chloride and magnesium sulphate); 48 h nutrient starvation (non-glucose, non-glutamine RPMI medium); or remained untreated (control). Cells were subsequently fixed, permeabilised and costained for AGR2 and the autophagosome marker SQSTM1, or AGR2 and the ER marker P4HB, then imaged on a confocal microscope (Fig. 9). SQSTM1-labelled autophagosomes were quantified and significantly increased numbers of autophagosomes per field of view and per cell were detected in the nutrient starved and H_2O_2 treated cells, compared to controls (Fig. 10). Salt stress did not significantly alter the number of autophagosomes visible. Thus, nutrient starvation and H_2O_2 treatment, but not salt stress treatment, appeared to stimulate autophagy as indicated by the significantly increased number of autophagosomes visible.

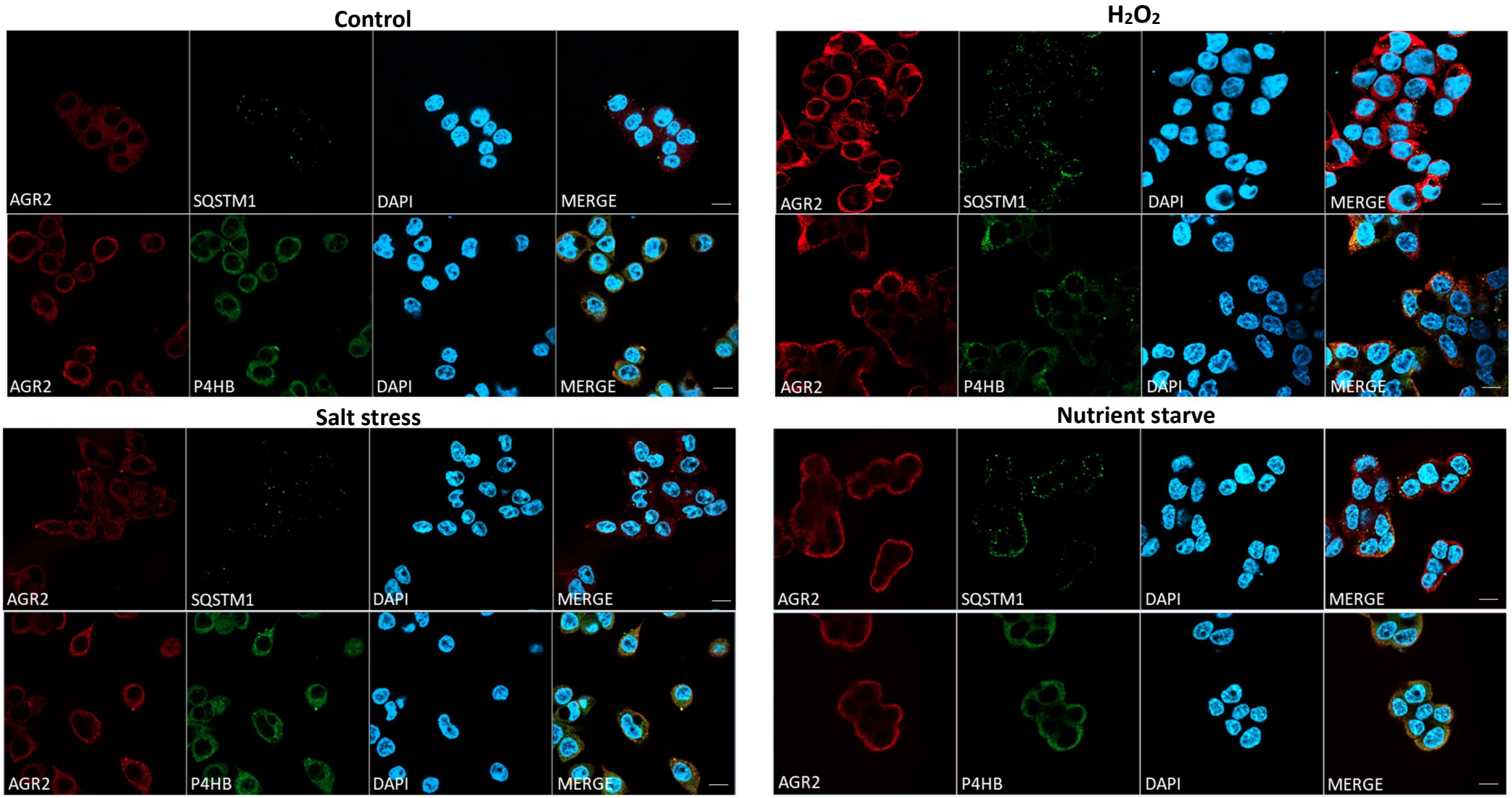

Figure 9. Intracellular distribution of AGR2 under stress conditions in OE19 cells. OE19 cells received 20 min H_2O_2 treatment (3mM); 48 h salt stress treatment (cultured in Earle's Balanced Salts Solution without calcium chloride and magnesium sulphate); 48 h nutrient starvation (non-glucose, non-glutamine RPMI medium); or remained untreated (control). After treatments, cells were fixed, permeabilised and stained for the colocalization of AGR2 (red) and either the autophagy receptor SQSTM1 (green) or the ER marker P4HB (green). Nuclei are stained for with DAPI. Slides were analysed on a Zeiss 800 confocal microscope at X63 magnification. Scale bar: 10 μm.

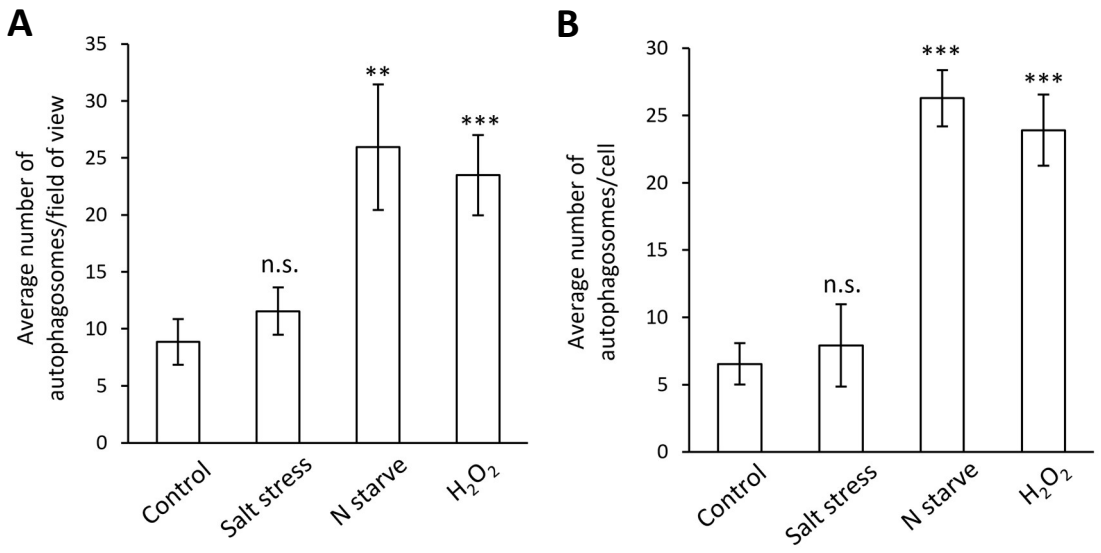

Figure 10. The ability of three stress treatments (salt stress, nutrient starvation, and H_2O_2 treatment) to stimulate autophagy in OE19 cells as assessed by immunofluorescence and quantification of the number of autophagosomes. Graphs represent the average number of autophagosomes per field of view **(A)** and per cell **(B)**. OE19 cells received the aforementioned treatments and were subsequently fixed, permeabilised and stained for the autophagosome marker SQSTM1. Slides were imaged on a Zeiss 800 confocal microscope at X63 magnification and the number of autophagosomes were counted manually using the ImageJ Counting Tool. Representative images used to generate autophagosome counts by staining for SQSTM1 are provided in Figure 9. Error bars represent standard deviation; n = 3; Unpaired t-tests, *P < 0.05, **P < 0.01, ***P < 0.005. n.s. - not significant. N starve - nutrient starvation.

Under the control and salt stress conditions, without significant autophagy stimulation, AGR2 localised with P4HB in the endoplasmic reticulum (Fig. 9) in accordance with previous findings (Fig. 6). In the nutrient-starved and H_2O_2-treated cells that did induce significant autophagy stimulation, there is some evidence to suggest that AGR2 localised further towards the plasma membrane (Fig. 9). Refer to Fig. 16 and Fig. 17 for follow-up experiments on AGR2 localisation with respect to the plasma membrane during nutrient starvation and oxidative stress. It is tempting to speculate that AGR2 may be capable of escaping the endoplasmic reticulum retrieval machinery under conditions of oxidative stress to interact with SQSTM1 and enable the stimulation of pro-survival autophagy. Such a role may involve AGR2 tracking towards the plasma membrane and being secreted, then being endocytosed back into the cell to interact with SQSTM1. This speculation, however, warrants further investigation. Furthermore, due to the tendency of these OE19 cells to grow in islands, it is also possible that the antibodies used could not permeate through to island centres. Such an effect could give the false impression of plasma membrane staining.

There is also some evidence of brighter AGR2 staining in nutrient-starved and H_2O_2-treated OE19 cells, compared to controls (Fig. 9). Therefore, SDS-PAGE and Western

blotting were used to investigate any potential change in the levels of AGR2 under these same cell stress conditions (nutrient starvation, salt stress and H_2O_2 treatment). SQSTM1 itself is degraded by autophagy, and thus decreased levels of this protein can be used as a marker of high autophagic flux (Bjørkøy *et al.,* 2009). Membranes were therefore stripped and reprobed for SQSTM1 to determine the level of autophagic flux during each of the cell stress treatments.

To verify that any potential changes to the levels of AGR2 and/or SQSTM1 from the cell stress treatments were due to autophagy stimulation, OE19 cells also received concomitant treatment with the autophagic inhibitor chloroquine during cell stress treatments. Chloroquine inhibits autophagy by blocking lysosomal acidification, thereby preventing autophagosome-lysosome fusion (Yoon *et al.,* 2010). A cytotoxicity evaluation of chloroquine in OE19 cells was carried out to identify a suitable concentration for use (Fig. 11). Chloroquine inhibited the viability of OE19 cells in a dose-dependent manner as tested by the Orangu assay, which measures the amount of formazan dye generated by dehydrogenases in living cells. To limit any potential reduction in cell viability, a maximum chloroquine concentration of 30 μM for 48 hours was used in the following experiments.

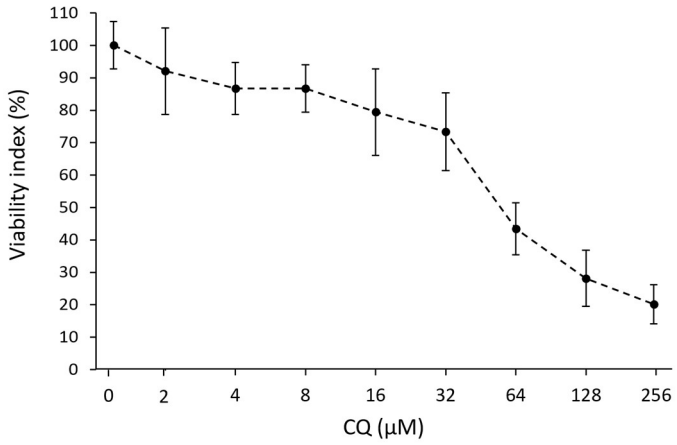

Figure 11. Cytotoxicity evaluation of chloroquine in OE19 cells. Cells were seeded at a density of 5 x 10^3 cells per well in a 96-well plate. Various concentrations of chloroquine (CQ) were added to cell cultures and cells were incubated for 48 h. Cell viability was assessed using the Orangu assay. Optical density values are normalised using the viability value of untreated cells (untreated cells = 100%). The results are mean ± SD of 3 experiments. CQ - chloroquine.

Figure 12 shows the levels of AGR2 and SQSTM1 in OE19 cells after 15 min H_2O_2 treatment, 24 h salt stress, and 24 h nutrient starvation and in untreated controls as determined by SDS-PAGE and Western blotting. No observable differences in the levels of AGR2 were induced by the cell stress treatments or from the same treatments +/-

chloroquine. Levels of SQSTM1 appeared to decrease slightly after 15 min H_2O_2 treatment, 24 h salt stress, and 24 h nutrient starvation, compared to the control, although these bands are not entirely clear potentially due to the SDS-PAGE gel becoming too hot.

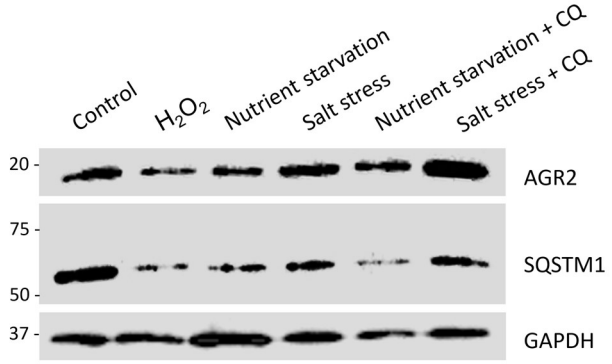

Figure 12. The effect of cell stress treatments on the levels of SQSTM1 and AGR2 in OE19 cells. OE19 cells either received 24 h salt stress treatment (cultured in Earle's Balanced Salts Solution without calcium chloride and magnesium sulphate); 24 h nutrient starvation (non-glucose, non-glutamine RPMI medium); 15 min H_2O_2 treatment (3mM); 24 h salt stress or nutrient starvation treatment concomitantly with 24 h chloroquine treatment (30 μM); or remained untreated (control). Cells were lysed and analysed by SDS-PAGE and reducing Western blotting with the ab76473 AGR2 mAb and the 66184-1-Ig SQSTM1 mAb. GAPDH was used as a loading control. CQ - chloroquine. kDa markers are shown.

OE19 cells subsequently received longer stress treatments (20 min H_2O_2 treatment, 48 h salt stress, and 48 h nutrient starvation) and the levels of AGR2 and SQSTM1 were assessed again using SDS-PAGE and Western blotting (Fig. 13). It is important to note that levels of AGR2 in the control lane appear as only a faint bad at 19 kDa because a lower overall protein concentration was loaded across all sample wells in these experiments (Fig. 13; Fig. 14). This was because lower protein concentrations were obtained when lysing cells under these cell stress conditions, potentially due to the removal of a higher proportion of unattached, dead cells.

The 20 min H_2O_2 treatment, 48 h nutrient starvation and 48 h salt stress treatments appeared to induce autophagy as indicated by reduced levels of SQSTM1 compared to the control (Fig. 13). These findings are in accordance with the increased number of autophagosomes that were observed upon 48 h salt stress and 48 h nutrient starvation, although no significant increase in the number of autophagosomes were observed during 48 h salt stress treatment (Fig 9; Fig. 10). The difference in the levels of SQSTM1 were cancelled out by chloroquine, indicating that treatment with 30 μM chloroquine for 48 h did indeed inhibit autophagy (Fig. 13). Interestingly, levels of AGR2 appeared to increase upon 20 min H_2O_2 treatment and 48 h nutrient starvation, compared to the control (Fig. 13). This increase in AGR2 appeared to be due to enhanced autophagy stimulation as

treating cells with chloroquine during H_2O_2 treatment or nutrient starvation reduced the levels of AGR2, as compared to the relevant stress treatment without chloroquine. This effect was particularly pronounced in the H_2O_2-treated OE19 cells.

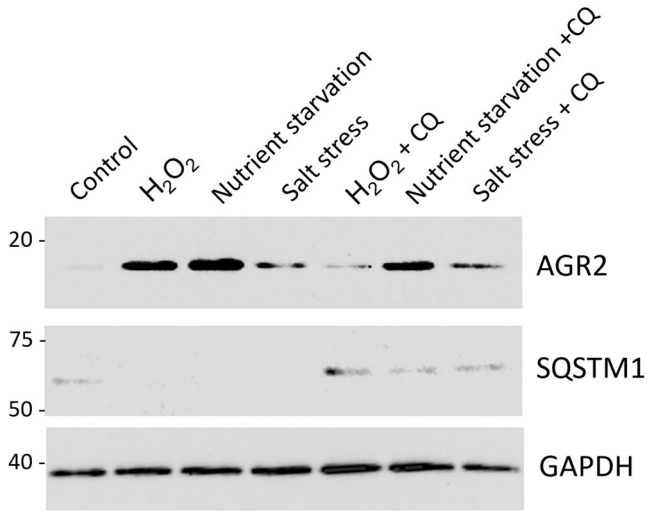

Figure 13. Levels of AGR2 increased during stress-induced autophagy stimulation in OE19 cells. OE19 cells received 20 min H_2O_2 treatment (3mM); 48 h nutrient starvation (non-glucose, non-glutamine RPMI medium); 48 h salt stress treatment (cultured in Earle's Balanced Salts Solution without calcium chloride and magnesium sulphate); 48 h chloroquine treatment (30 μM) followed by 20 min H_2O_2 treatment (3 mM); 48 h salt stress or nutrient starvation treatment concomitantly with 48 h chloroquine treatment (30 μM); or remained untreated (control). Cells were lysed and analysed by SDS-PAGE and reducing Western blotting with the ab76473 AGR2 mAb and the 66184-1-Ig SQSTM1 mAb. GAPDH was used as a loading control. CQ - chloroquine. kDa markers are shown.

To validate the aforementioned findings, the levels of AGR2 under the same cell stress conditions (+/- chloroquine) were assessed by SDS-PAGE and Western blotting in triplicate and subsequently quantified by densitometry using ImageJ (Fig. 14). The levels of AGR2 significantly increased in the OE19 cells during 20 min H_2O_2 treatment and 48 h nutrient starvation, compared to untreated controls. When treated concomitantly with chloroquine, the levels of AGR2 did not significantly increase during any cell stress treatment compared to controls. This finding suggests that the increase in AGR2 appeared to be due to increased autophagy stimulation.

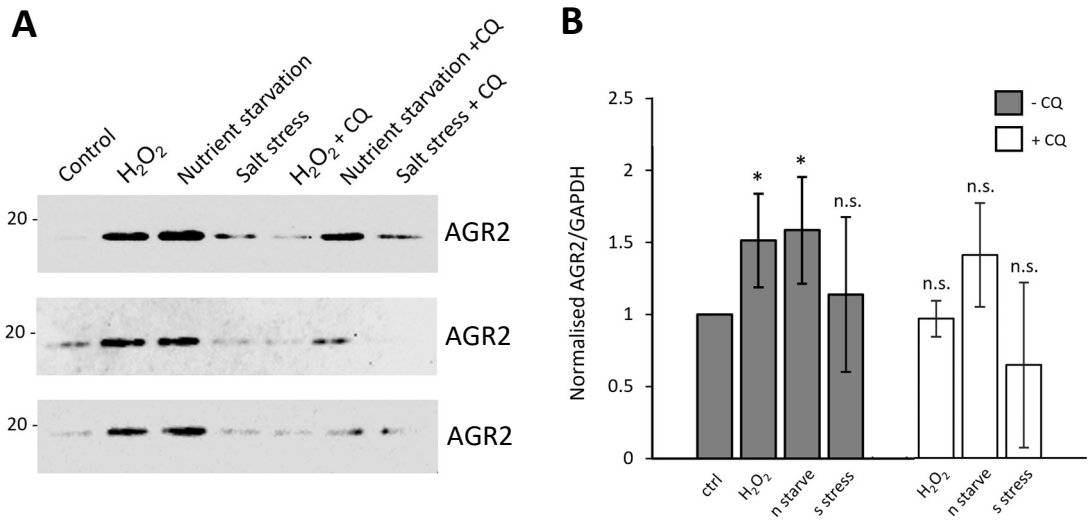

Figure 14. Levels of AGR2 significantly increase during 20 min H_2O_2 treatment and 48 h nutrient starvation. OE19 cells received 20 min H_2O_2 treatment (3mM); 48 h nutrient starvation (non-glucose, non-glutamine RPMI medium); 48 h salt stress treatment (cultured in Earle's Balanced Salts Solution without calcium chloride and magnesium sulphate); 48 h chloroquine treatment (30 μM) followed by 20 min H_2O_2 treatment (3 mM); 48 h salt stress or nutrient starvation treatment concomitantly with 48 h chloroquine treatment (30 μM); or remained untreated (controls). Cells were lysed and analysed by SDS-PAGE and reducing Western blotting in triplicate with the ab76473 AGR2 mAb **(A)**. Levels of AGR2 were quantified by densitometry using ImageJ software (**B**). Error bars represent standard deviation; n = 3; Unpaired t-tests, *P < 0.05, **P < 0.01, ***P < 0.005. n.s. - not significant; CQ - chloroquine; ctrl - control; n starve - nutrient starve; s stress - salt stress. kDa markers are shown.

Immunofluorescence evidence suggested that AGR2 may localise at the plasma membrane during 48 h nutrient starvation and 20 min H_2O_2 treatment (Fig. 9). To explore this notion, it was necessary to identify a marker of the plasma membrane in the OE19 cells. Therefore, after 48 h nutrient starvation, 20 min H_2O_2 treatment or under control conditions, OE19 cells were incubated for 15 minutes in RPMI medium containing 7 μg/ml CellMask Deep Red plasma membrane stain (C10046). Cells were subsequently imaged live with a Zeiss 880 laser scanning confocal microscope. CellMask appeared to effectively label the plasma membrane in the OE19 cells during live-cell imaging under the control, H_2O_2 treatment and nutrient starvation conditions (Fig. 15).

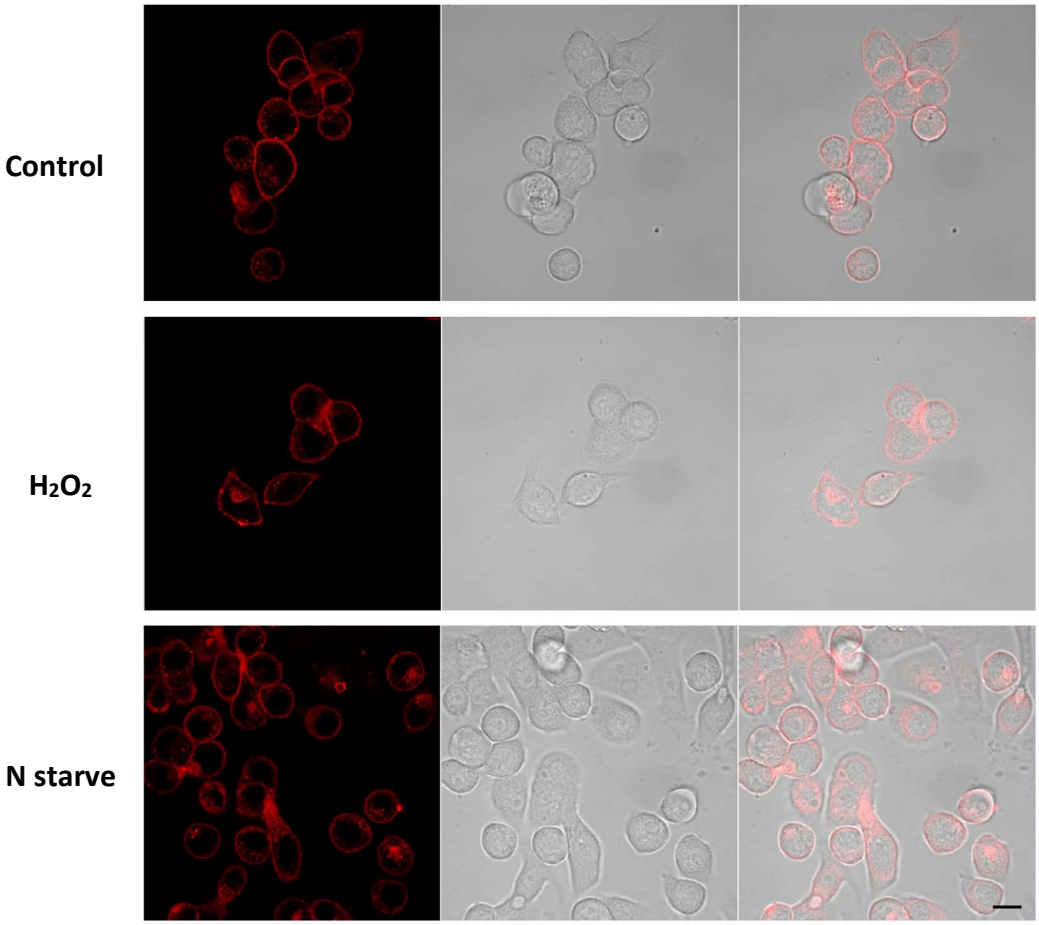

Figure 15. Live-cell labelling of the plasma membrane using CellMask in OE19 cells. Cells either remained untreated (control); received H_2O_2 treatment (3mM, 20 min); or underwent nutrient starvation (48 h incubation in non-glucose, non-glutamine RPMI medium). After treatments, cells were incubated at 37°C in the presence of 5% CO_2 for 15 minutes in RPMI medium containing 7 µg/ml CellMask™ Deep Red plasma membrane stain (C10046). Cells were washed twice with fresh RPMI and then imaged with a Zeiss 880 laser scanning confocal microscope at X 63 magnification. Scale bar: 10 µm. N starve – nutrient starvation.

After CellMask was established as a suitable plasma membrane stain for OE19 cells by live-cell imaging, fixed-cell imaging was used to explore any potential colocalization of AGR2 and CellMask during 48 h nutrient starvation. CellMask staining (red) appeared more diffuse when used in fixed-cell imaging (Fig. 16) compared to live-cell imaging (Fig. 15), making it less suitable as a plasma membrane marker for this purpose. However, the images obtained still suggested that AGR2 (green) localised closer to the plasma membrane in the nutrient starved cells, compared to the control cells (Fig. 16). It is worthy to note that the relatively small size and roundness of these OE19 cells may give a false impression or heightened appearance of plasma membrane staining.

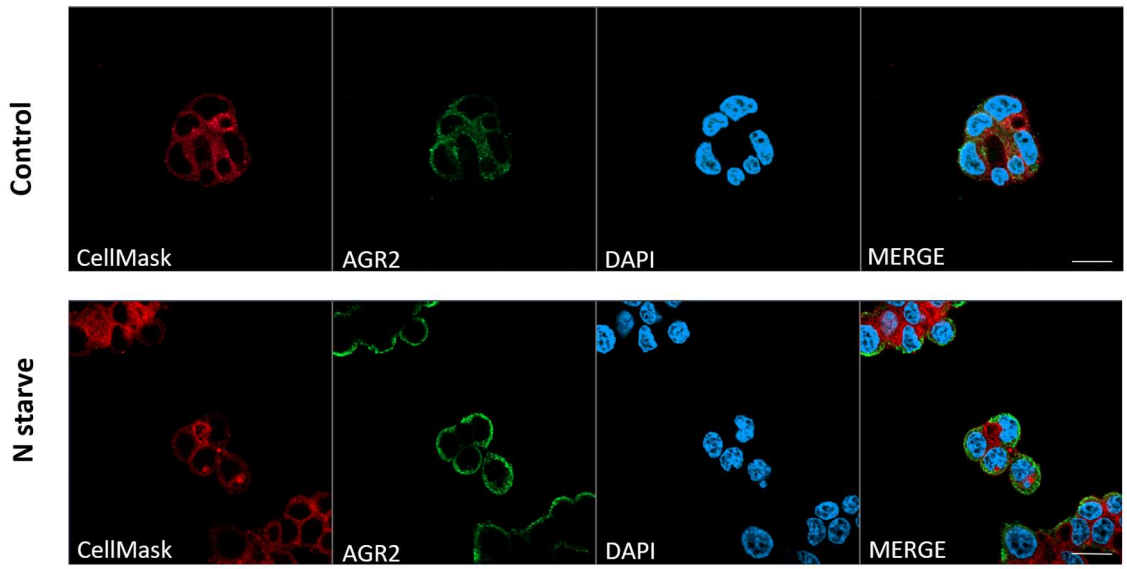

Figure 16. Distribution of AGR2 (green) during 48 h nutrient starvation in OE19 cells stained with the plasma membrane marker CellMask (red). Cells underwent nutrient starvation (48 h incubation in non-glucose, non-glutamine RPMI medium) or remained untreated (control). After treatment, cells were incubated at 37°C in the presence of 5% CO_2 for 15 minutes in RPMI medium containing 7 µg/ml CellMask™ Deep Red plasma membrane stain (C10046). Cells were washed twice with fresh RPMI and subsequently fixed and stained for the expression of AGR2. Nuclei were stained with DAPI. Images were taken on a Zeiss LSM 800 confocal microscope at X63 magnification. Scale bar: 10 µm. N starve - nutrient starvation.

Fixed-cell imaging was subsequently used to explore any potential colocalization between AGR2 and CellMask during treatment with H_2O_2. OE19 cells were treated with 3mM H_2O_2 for 0, 15 or 30 mins to investigate any potential changes to the localisation of AGR2 that may occur incrementally with increasing exposure to oxidative stress. OE19 cells were also concomitantly incubated with 7 µg/ml CellMask for 10, 20 or 30 mins to ascertain the optimal treatment time for plasma membrane staining during fixed-cell imaging. Optimal plasma membrane labelling appeared to occur at 10 min incubation with CellMask, although staining still appeared diffuse at this timepoint (Fig. 17). It is thus apparent that part of the cell fixing process interferes with the precise labelling of the plasma membrane using the CellMask stain. Interestingly, as periods of H_2O_2 treatment lengthened, an increasing aggregation-promoting effect on AGR2 was observed. Indeed, the number of AGR2 aggregates were quantified and significantly more AGR2 aggregates were observed per cell and field of view following each incremental increase in H_2O_2 treatment time from 10 to 30 mins (Fig. 18).

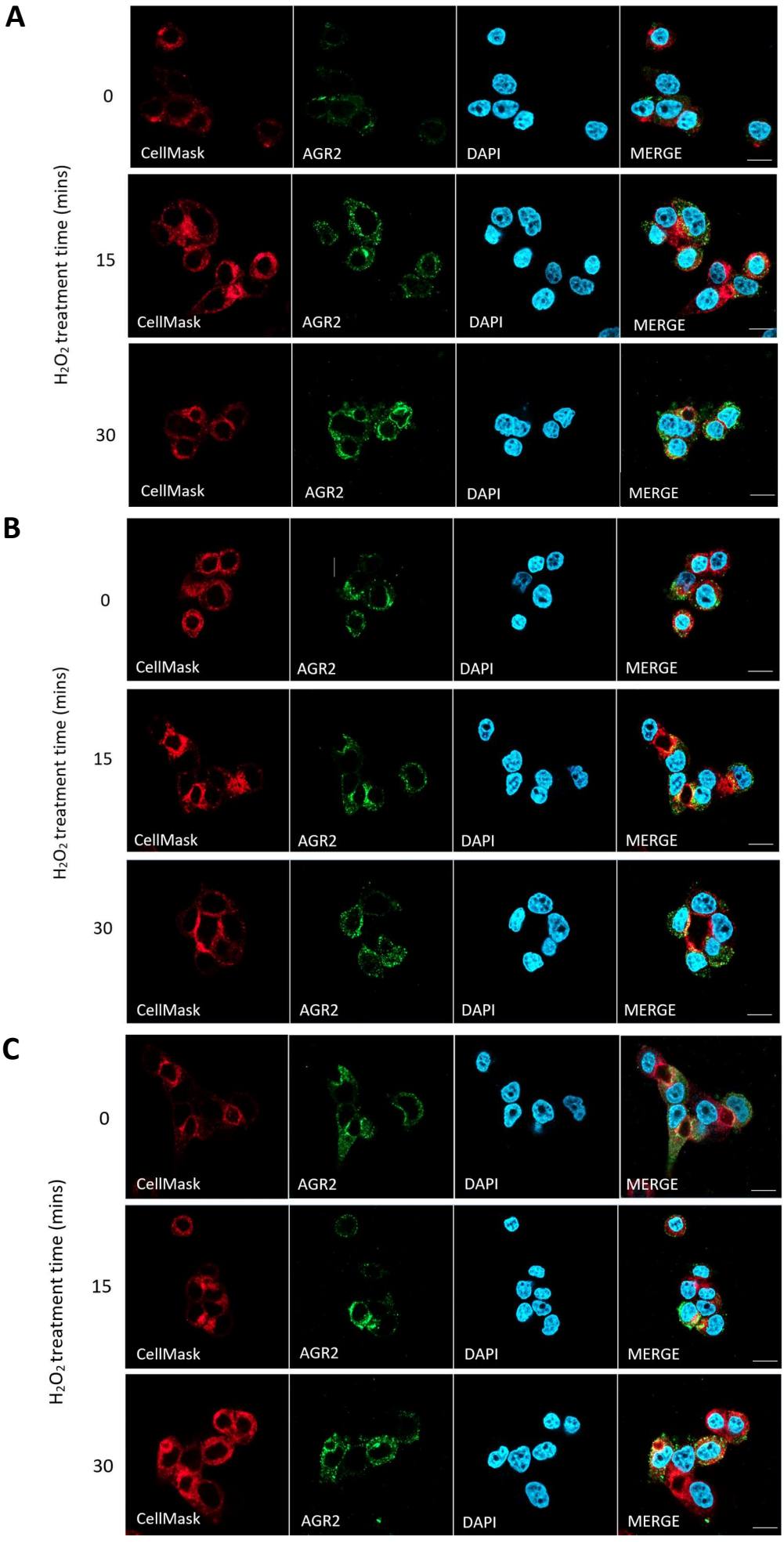

Figure 17. Distribution of AGR2 (green) following H_2O_2 treatment in OE19 cells stained with CellMask (red). Cells were incubated at 37°C in 5% CO_2 for 10 **(A)**, 20 **(B)** or 30 **(C)** mins in RPMI medium containing 7 µg/ml CellMask™ Deep Red plasma membrane stain (C10046). After treatment, cells were washed once in fresh RPMI medium and subsequently treated with 3mM H_2O_2 in RPMI medium for 0, 15, or 30 mins at 37°C in 5% CO_2. Cells were then washed three times in PBS++, fixed, and stained for the expression of AGR2. Nuclei were stained with DAPI. Images were taken on a Zeiss LSM 800 confocal microscope at X63 magnification. Scale bar: 10 µm.

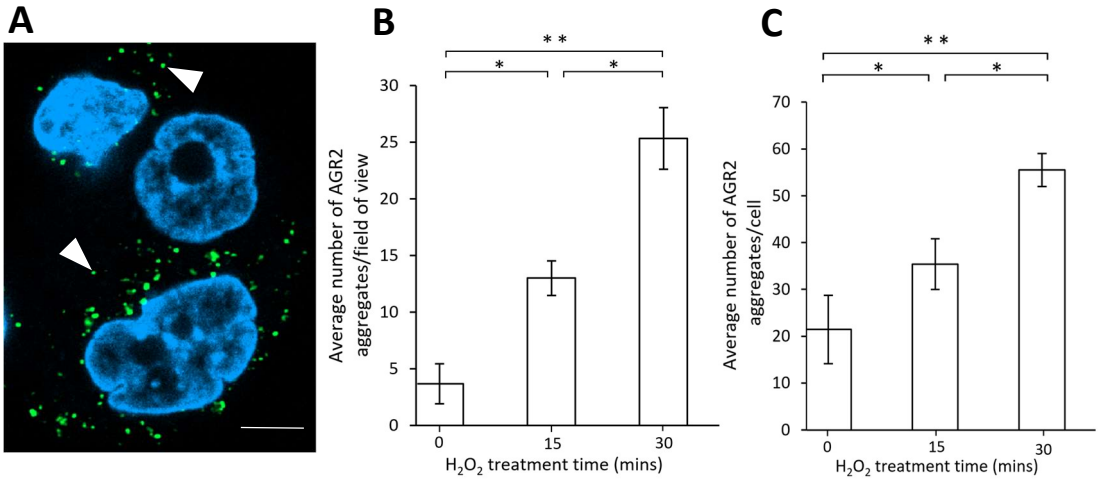

Figure 18. Significantly more AGR2 aggregates are observed per cell and field of view following increases in exposure time to oxidative stress. A representative confocal image of OE19 cells that were treated with 3 mM H_2O_2 for 15 min, washed, fixed and stained for the expression of AGR2 (green) **(A).** Arrowheads show examples of AGR2 aggregates. Nuclei were stained for with DAPI. Scale bar: 5 µm. The number of AGR2 aggregates were quantified per field of view **(B)** and per cell **(C)** following 0, 15 and 30 min H_2O_2 treatment (3 mM). Error bars represent standard deviation; n = 3; Unpaired t-tests, *P < 0.05, **P < 0.01, ***P < 0.005.

The AGR2 aggregates observed in Figure 17 and 18A appeared similar in shape (circular) and size (~0.5 µm) to suggest they may be present within autophagosomes. However, little colocalization was observed previously between AGR2 and the autophagosome marker SQSTM1 following 20 min treatment with 3 mM H_2O_2 (Fig. 9). To further investigate the aggregation-promoting effect of H_2O_2 treatment on AGR2, immunofluorescence was used to explore any potential colocalization between AGR2 and another autophagosome marker known as LC3 following 0, 10, 20 and 30 min treatments with 3 mM H_2O_2. LC3 plays a role in the selection of substrates for autophagy and in autophagosome biogenesis and may show differential staining to SQSTM1 (Rogov *et al.,* 2014). The number of LC3-labelled autophagosomes increased with longer exposure to H_2O_2, indicating an increase in autophagy stimulation (Fig. 19). An aggregation-promoting effect on AGR2 was again observed with increasing H_2O_2 exposure (Fig. 19), corresponding to previous findings (Fig. 17). Analogously to nutrient starvation treatment (Fig. 9; Fig. 16), many of these AGR2 aggregates were observed in close proximity to the plasma membrane (Fig. 19). Importantly, AGR2 aggregates did not show clear colocalization with the LC3-labelled autophagosomes (Fig. 19). Therefore, other factors are likely to account for the observed aggregation of AGR2, including perhaps its enclosure in vesicles or an association with mucin complexes.

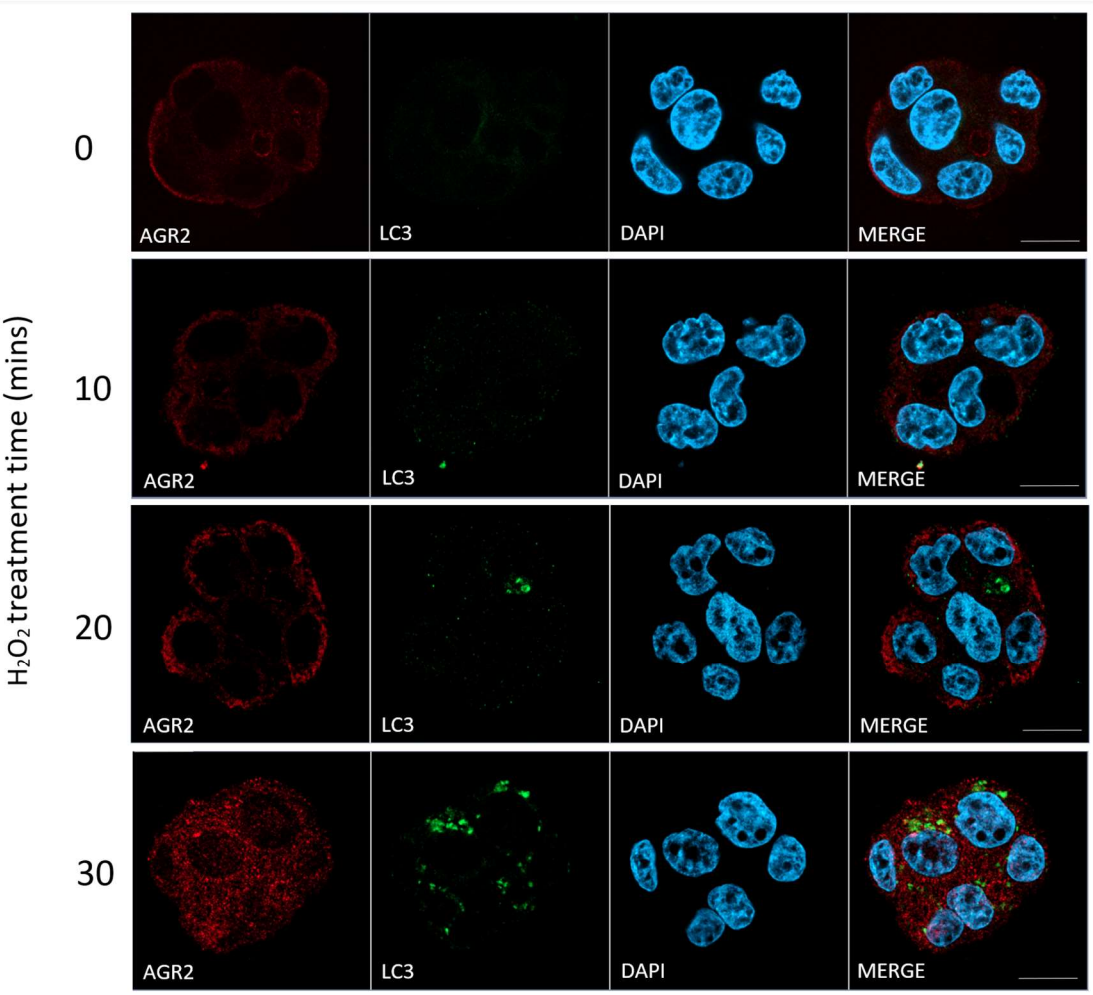

Figure 19. Intracellular distribution of AGR2 (red) and LC3 (green) in OE19 cells following increasing periods of H_2O_2 exposure. OE19 cells were exposed to 0, 10, 20 and 30 min H_2O_2 treatment (3mM). After treatments, cells were fixed, permeabilised and stained for the colocalization of AGR2 and LC3. Nuclei are stained for with DAPI. Images were taken on a Zeiss LSM 800 confocal microscope at X63 magnification. Scale bar: 10 µm.

3.5. AGR2 is secreted from OE19 cells

Given that AGR2 localises in close proximity to the plasma membrane following nutrient starvation and H_2O_2 treatment, and that AGR2 plays a known role in the tumour microenvironment, it seemed prudent to investigate any potential secretion of AGR2 from the OE19 cells. OE19 cells received 20 min H_2O_2 treatment (3mM), 48 h nutrient starvation, or remained untreated as controls. Culture media were collected and subjected to SDS-PAGE and Western blotting with the ab76473 AGR2 mAb. It is worthy to note that a high overall protein concentration of 50 µg (as measured by the BSA protein assay) were loaded into wells from each sample of culture media. Figure 20 shows that AGR2 was detected in relatively equal concentrations in the media collected from the control, H_2O_2-stressed and nutrient-starved OE19 cells. Therefore, the cell stress treatments did

not appear to induce an increase in AGR2 secretion. The presence of extracellular AGR2 in the culture media also demonstrates that AGR2 is likely to be present at the plasma membrane of OE19 cells under the control and cell stress conditions, as was debated previously (Fig. 9; Fig. 16; Fig. 17). The extracellular function of AGR2 and the mechanism by which it escapes the endoplasmic reticulum retrieval machinery remain undetermined and warrant further investigation.

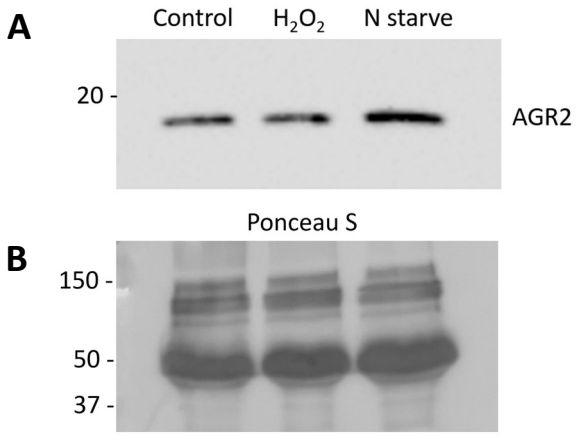

Figure 20. AGR2 is secreted from OE19 cells under control, H_2O_2-stressed and nutrient-starved conditions. OE19 cells received 20 min H_2O_2 treatment (3mM); 48 h nutrient starvation (non-glucose, non-glutamine RPMI medium); or remained untreated (control). Culture media were collected 72 h after cells were last split and subjected to SDS-PAGE and Western blotting with the ab76473 AGR2 mAb (**A**). Cells were lysed at a confluency of 8.9 x 10^6. Ponceau S staining was used as a loading control (**B**). kDa markers are shown. N starve – nutrient starvation.

In the conventional secretory pathway, proteins utilise a N-terminal signal sequence to enable translocation into the endoplasmic reticulum and subsequent targeting to the Golgi then plasma membrane via secretory vesicles or granules (Vitale and Denecke, 1999). Importantly, proteins show a high degree of variation in signal sequence conservation and length (Hiller *et al.,* 2004). Other proteins may use unconventional protein secretion, which does not require an N-terminal signal sequence or involve transport through the endoplasmic reticulum and Golgi (Kim, Gee and Lee, 2018). The mechanism by which AGR2 is secreted from cancer cells remains undetermined. To investigate the potential for AGR2 to follow the conventional secretory pathway, the PrediSi (Prediction of Signal Peptides) tool was used to determine the presence of a signal peptide from the human AGR2 amino acid sequence. This computational tool uses a position weight matrix approach based on the frequency of amino acids in parts of the signal sequences from constructed datasets (Hiller *et al.,* 2004). This calculation also includes a frequency correction that takes into account the amino acid bias in proteins. A predicted signal

peptide was identified in the N-terminus of AGR2 with 96% confidence (Fig. 21A). The predicted signal peptide was 20 amino acids in length from Met1-Ala20 (Fig. 21B). The presence of this predicted signal peptide in AGR2 suggests that AGR2 may follow the conventional secretory pathway rather than the unconventional one.

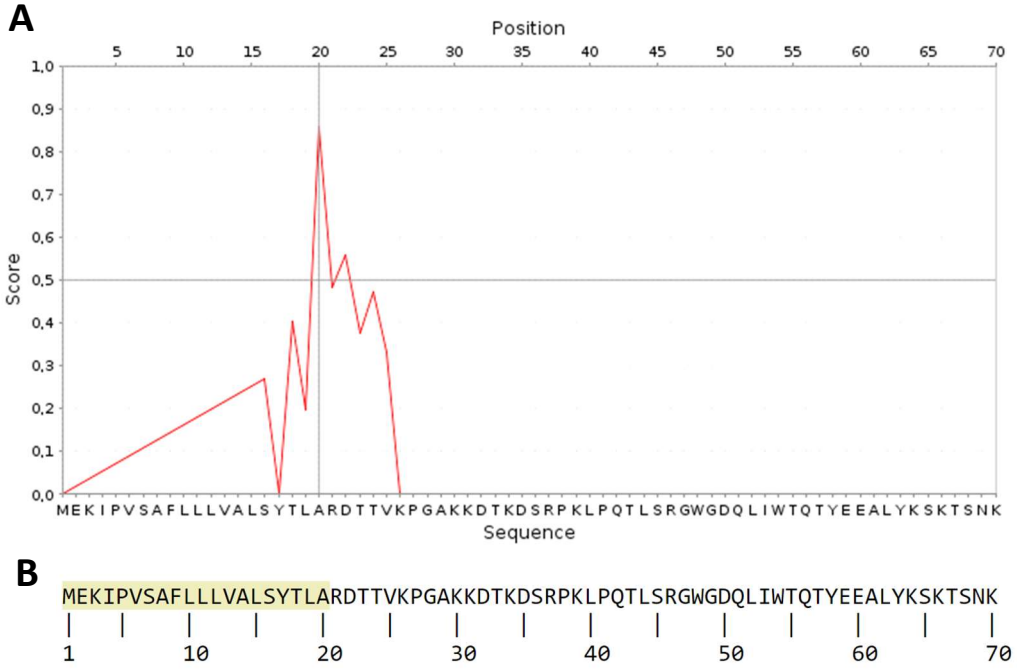

Figure 21. PrediSi predicted the presence of a signal peptide from Met1-Ala20 in AGR2. The score represents statistical ideal amino acid frequency for each position in the amino acid sequence along the human AGR2 protein (**A**). The signal peptide (highlighted in yellow) is predicted to be cleaved off between Ala20 and Arg21 (**B**). The signal peptide was predicted with 96% confidence.

3.6. Cytotoxicity evaluation of the autophagy inhibitor chloroquine in OE19 and OE33 cells

To finalise these experiments, the extent to which the OE19 cells may utilise autophagy to promote cellular survival required investigation. Figure 5 demonstrated that AGR2 is strongly expressed in OE19 cells, but is not detectable by Western blotting in OE33 cells. The availability of two oesophageal adenocarcinoma cell lines in which one expresses AGR2 (OE19 cells) and one does not (OE33 cells) provides a system to compare the extent to which cells may potentially rely on AGR2-associated autophagy for cellular survival. Therefore, a cytotoxicity evaluation of the autophagy inhibitor chloroquine was carried out in these two cell lines.

Chloroquine inhibited the viability of the OE19 and OE33 cells in a dose-dependent manner as tested by the Orangu assay (Fig. 22). The OE19 cells were more sensitive to chloroquine compared with the OE33 cells; the CC_{50} (50% cytotoxic concentration) was

determined as 56 μM in OE19 cells and 103 μM in OE33 cells. To our knowledge, the CC_{50} of chloroquine in OE19 or OE33 cells has not previously been reported. Images of cells at each concentration of chloroquine were taken using the EVOS Cell Imaging System and further demonstrate the increased sensitivity of the OE19 cells to chloroquine, compared to the OE33 cells (Fig. 22A). The increased sensitivity of the AGR2-expressing OE19 cells to autophagy inhibition provides evidence to support future knockout studies exploring the potential role of AGR2 in pro-survival autophagy, particularly under oxidative stress conditions. It is important to note that many other inter-tumour differences between the OE19 and OE33 cell lines that have not been explored here could also underly the variation in chloroquine sensitivity.

Numerous studies have reported the anticancer potential of chloroquine when used as a monotherapy or in combination with chemotherapy across a range of different tumour types (Joshi *et al.,* 2012; Maycotte *et al.,* 2015; Hu *et al.,* 2016; Eloranta *et al.,* 2020). However, the efficacy of chloroquine in cancers of the oesophagus has not previously been reported. The reduced viability of the OE19 and OE33 cell lines from concentrations of chloroquine in the micromolar range supports further investigation into the potential therapeutic benefits of chloroquine for oesophageal adenocarcinoma.

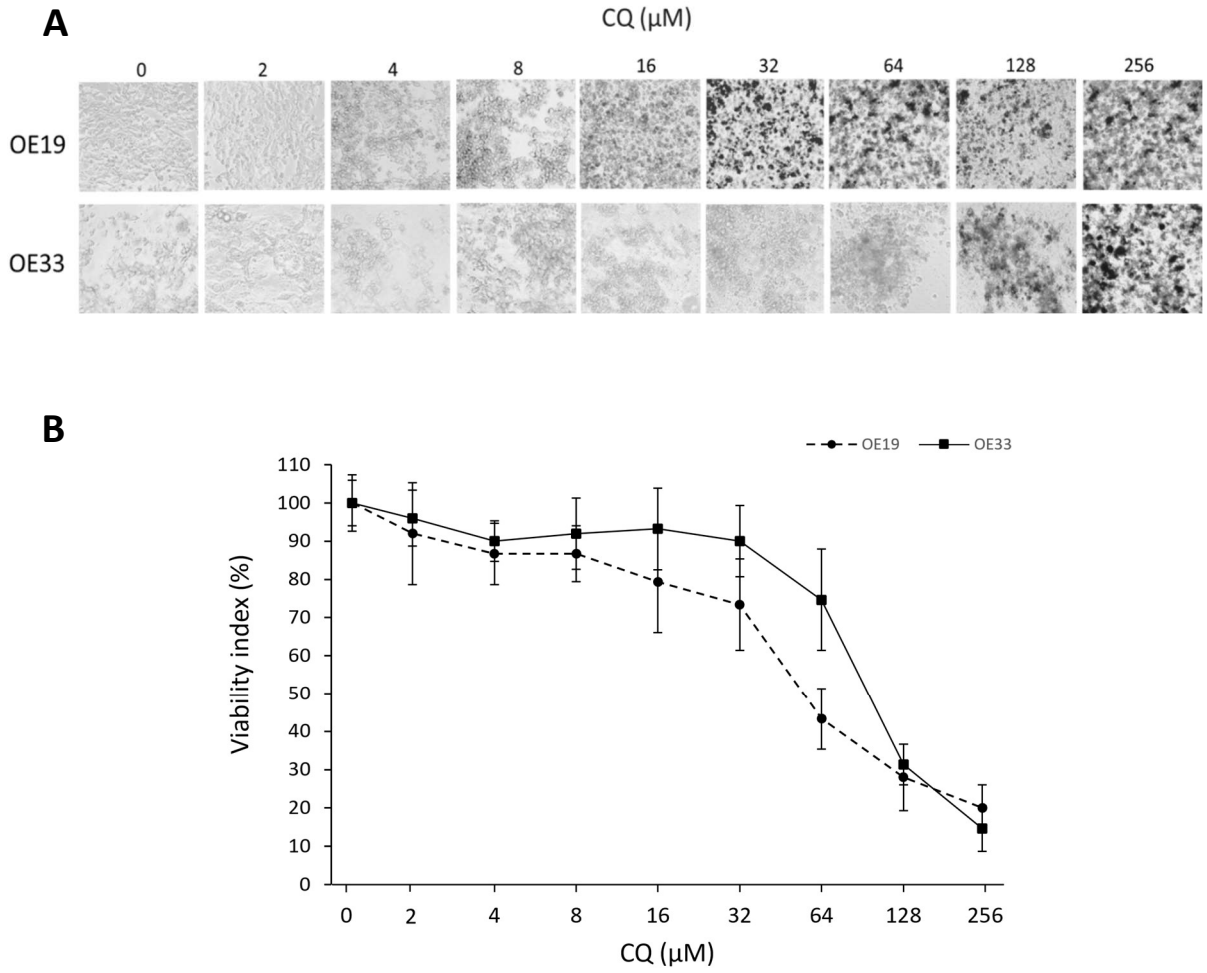

Figure 22. Cytotoxicity evaluation of chloroquine in OE19 and OE33 cells. Cells were seeded at a density of 5 x 10^3 cells per well in a 96-well plate. Various concentrations of chloroquine were added to cell cultures and cells were incubated for 48 h. Images obtained using the EVOS Cell Imaging System at 40x magnification **(A)**. Cell viability was assessed using the Orangu assay **(B)**. Optical density values are normalised using the viability value of untreated cells (untreated cells = 100%). The results are mean ± SD of 3 experiments. Chloroquine - CQ.

3.7. Summary of results

Reducing and non-reducing SDS-PAGE followed by Western blotting demonstrated that AGR2 forms disulphide-dependent complexes in OE19 cells, but AGR2 could not be detected in the OE21 or OE33 cells (Fig. 5). The interaction between AGR2 and SQSTM1, first identified by Worfolk *et al.* (2019), was then verified by immunoprecipitation experiments (Fig. 7). Immunofluorescence experiments showed that the majority of AGR2 appeared to colocalise with P4HB in the endoplasmic reticulum (Fig. 6). However, there was some evidence to suggest that AGR2 localised further towards the plasma membrane in the OE19 cells during nutrient starvation and H_2O_2 treatment (Fig. 9). Both nutrient starvation and H_2O_2 treatment were capable of inducing autophagy in OE19 cells

as demonstrated by significantly increased numbers of autophagosomes and reduced levels of SQSTM1 (Fig. 10; Fig. 13). Although there was not clear colocalization between AGR2 and SQSTM1 under control or autophagy-inducing conditions, some areas of overlap were visible (Fig. 8; Fig. 9). Levels of AGR2 were found to significantly increase following nutrient starvation and H_2O_2 treatment (Fig. 14). This increase in the levels of AGR2 appeared to be due to enhanced autophagy stimulation as treating cells with chloroquine during H_2O_2 treatment or nutrient starvation reduced the levels of AGR2 (Fig. 13; Fig. 14). The short 20-min time frame in which AGR2 levels increased during the H_2O_2 treatment suggests a potential reduction in the proteolytic degradation of AGR2, possibly as part of a pro-survival autophagy response to oxidative stress conditions. Interestingly, as periods of H_2O_2 treatment lengthened, an increasing aggregation-promoting effect on AGR2 was observed (Fig. 17; Fig. 18). However, AGR2 aggregates did not show clear colocalization with LC3-labelled autophagosomes (Fig. 19). Therefore, other factors are likely to account for the observed aggregation of AGR2, including its potential enclosure in vesicles or an association with mucin complexes.

AGR2 was shown to be secreted into the culture media from OE19 cells (Fig. 20). AGR2 was detected in relatively equal concentrations in the media collected from control, H_2O_2-stressed and nutrient-starved OE19 cells (Fig. 20). Thus, cell stress treatments did not appear to induce an increase in AGR2 secretion. The presence of a predicted signal peptide in AGR2 suggests that AGR2 follows the conventional secretory pathway rather than the unconventional one (Fig. 21). Lastly, chloroquine inhibited the viability of the OE19 and OE33 cells in a dose-dependent manner as tested by the Orangu assay (Fig. 22), supporting future studies investigating the therapeutic potential of autophagy inhibition for oesophageal adenocarcinoma. AGR2 expressing OE19 cells were more sensitive to chloroquine compared with AGR2 non-expressing OE33 cells; the CC_{50} was determined as 56 μM and 103 μM in the OE19 and OE33 cells, respectively (Fig. 22).

4. Discussion

4.1. AGR2 interacts with its client proteins through disulphide bonds

In the present study, AGR2 was strongly expressed in OE19 cells but was not detectable by Western blotting in OE21 and OE33 cells (Fig. 5). AGR2 expression is normally restricted to specific secretory and reproductive organs. However, AGR2 is found derepressed in various cancers, including individual cases of oesophageal adenocarcinoma. The difference in AGR2 expression between these three oesophageal adenocarcinoma cell lines thus highlights the heterogeneity of tumour gene expression. These findings suggest that should AGR2 play a functional role in pro-survival autophagy, it is not ubiquitously required in oesophageal adenocarcinoma. Indeed, individual tumours of the same type frequently do not follow the same evolutionary pathway in terms of the oncogenic aberrations accumulated during tumour progression (Ciriello and Magnani, 2021). However, it would also be worthwhile to utilise more sensitive methods (e.g. RNA sequencing or mass spectrometry) to investigate whether AGR2 is potentially being expressed in the OE21 and OE33 cells at a level below the limit of detection by Western blotting.

A proteomics screen identified AGR2 as a protein that is universally upregulated in Barrett's oesophagus, a premalignant condition for the development of oesophageal adenocarcinoma (Pohler *et al.,* 2004). It would therefore be interesting to investigate any potential survival advantage AGR2 may specifically convey to the highly inflammatory and metaplastic environment present during Barrett's oesophagus, and its progression to oesophageal adenocarcinoma. In breast cancer, the overexpression of AGR2 is a predicter of poor prognosis (Hrstka *et al.,* 2010); however, it remains to be determined whether this is also the case in oesophageal adenocarcinoma.

AGR2 is an evolutionary distant member of the PDI family of proteins and possesses a single cysteine residue in its thioredoxin-like domain (residues CPHS). Using SDS-PAGE and Western blotting, it was shown that AGR2 complexes in the OE19 cell lysates were dispersed by the addition of DTT, and thus are disulphide dependent (Fig. 5). Therefore, it is clear that endogenous AGR2 can form disulphide dependent complexes in OE19 cells through its single cysteine residue. This is in accordance with studies showing that, through its single cysteine residue, AGR2 forms mixed disulphides with the mucins MUC1, MUC2 and MUC5AC (Park *et al.,* 2009; Schroeder *et al.,* 2012; Norris *et al.,*

2013). Through its non-canonical CPHS domain, AGR2 can also form disulphide bonds with itself, creating homodimers (Clarke *et al.,* 2016).

The mechanism by which AGR2 mediates disulphide bond formation with its client proteins is currently unclear as AGR2 lacks a redox active thioredoxin motif with dual cysteines. It has been suggested that the dimeric structure of AGR2 may permit disulphide bond formation by providing a redox capacity equivalent to the canonical thioredoxin motif with dual cysteines (Moidu *et al.,* 2020). Indeed, the dissociation constant of dimerization indicates that AGR2 is in its dimeric state in the endoplasmic reticulum (Patel *et al.,* 2013). It is also plausible that additional redox enzymes in the endoplasmic reticulum may be involved in assisting AGR2 to perform full redox reactions. For instance, AGR2 is known to form mixed disulphides with MUC2 (Park *et al.,* 2009), but perhaps another oxidation enzyme is required to complete disulphide bond formation within this mucin. Several redox enzymes are known to act cooperatively to enable disulphide bond formation in the endoplasmic reticulum, such as the endoplasmic reticulum oxidoreductin 1-protein disulphide isomerase (ERO1-PDI) oxidation pathway (Araki and Inaba, 2012). Moreover, through immunoprecipitation followed by mass spectrometry experiments, AGR2 has been shown to interact with various other endoplasmic reticulum chaperone proteins that include Ero1α, ERp29, ERp44 and peroxiredoxin IV (Worfolk *et al.,* 2019). Another possibility is that although the absence of dual cysteines may hinder AGR2 from oxidising disulphide bonds in its client proteins, the single cysteine residue in its CPHS domain may allow for the isomerisation of necessary disulphide bonds (Fig. 1). By mediating the rearrangement of disulphide bonds, AGR2 could perhaps play a vital role in stabilising the structure of the large and complex mucins.

Wofolk *et al.* (2019) lysed OE19 cells in the presence or absence of N-Ethylmaleimide (NEM), which blocks sulphydryl groups to prevent disulphide bond formation. The authors then used immunoprecipitation followed by mass spectrometry to identify disulphide-dependent AGR2 interacting proteins. SQSTM1 was identified as an AGR2 interacting protein that was detected only when cells were lysed in the absence of NEM, demonstrating that this interaction was disulphide-dependent. The present study verified the interaction between AGR2 and SQSTM1 in OE19 cells by immunoprecipitation followed by SDS-PAGE and Western blotting (Fig. 7). The notion that AGR2 may be involved in autophagy was founded upon three key points: firstly, that disulphide bond formation is known to be required in SQSTM1 to stimulate pro-survival autophagy

(Carroll *et al.,* 2018); secondly, that AGR2 is known to be involved in mucin disulphide bond formation (Park *et al.,* 2009); and lastly, that a disulphide-dependent interaction exists between AGR2 and SQSTM1 (Worfolk *et al.,* 2019). It is plausible, therefore, that the upregulation of SQSTM1 and AGR2 in human cancers could be involved in the induction of pro-survival autophagy.

4.2. A potential oncogenic role for AGR2 in pro-survival autophagy

Genomic alterations in AGR2 and SQSTM1 were investigated in cBioPortal using the data from the Pan-Cancer Analysis of Whole Genomes (PCAWG) containing 2,683 samples and 2,565 patients (The ICGC/TCGA Pan-Cancer Analysis of Whole Genomes Network, 2020). AGR2 amplification was the prominent genomic alteration identified across various cancers in this dataset (Fig. 23A). It therefore holds that AGR2 is overexpressed in cancer for its oncogenic function and that AGR2 mutants play a much smaller role in tumorigenesis. Analogously, SQSTM1 amplification was a frequent genomic alteration across many cancers in this dataset (Fig. 23B), emphasising the role of autophagy in tumour initiation and progression (Lu, He and Ma, 2020).

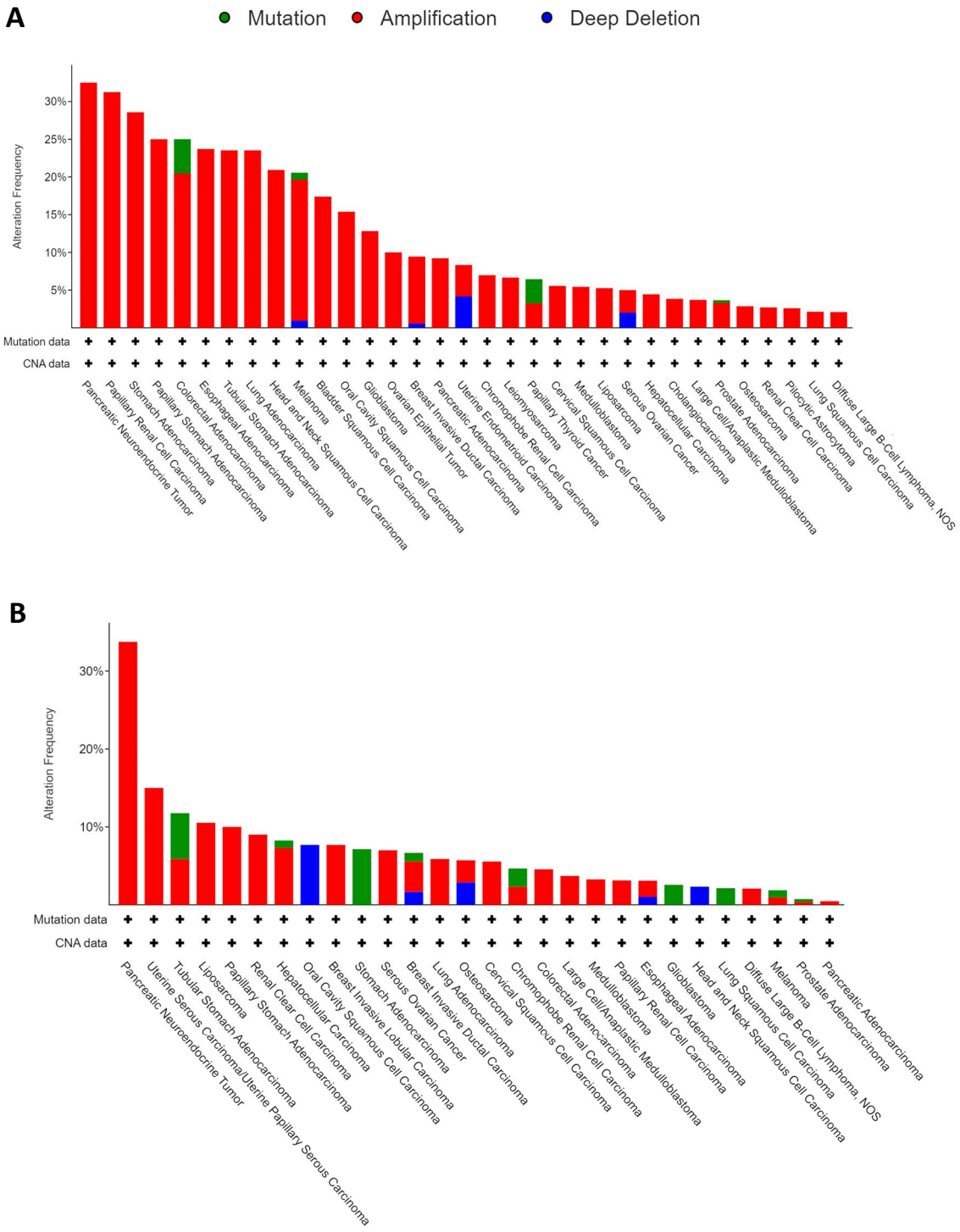

Figure 23. Genomic alterations of AGR2 (A) and SQSTM1 (B) across data from the Pan-Cancer Analysis of Whole Genomes Consortium of the International Cancer Genome Consortium (ICGC) and The Cancer Genome Atlas (TCGA) (The ICGC/TCGA Pan-Cancer Analysis of Whole Genomes Network, 2020). Database contains 2683 samples/2565 patients with mutation and copy number alteration data. Analysis was carried out in cBioPortal (https://www.cbioportal.org/).

Autophagy is an important mechanism for the degradation of proteins and organelles that have been damaged by oxidative stress and may be toxic to the cell (Filomeni, Zio and Cecconi, 2015). Tumours are exposed to high levels of oxidative stress due to impaired perfusion and heightened proliferation; therefore, autophagy can prevent cytotoxicity in cancer environments (Taucher *et al.,* 2022). Furthermore, through the degradation and recycling of proteins and organelles, enhanced autophagy stimulation can serve to maintain nutrient supplies to rapidly dividing tumour cells (He *et al.,* 2018). By ameliorating oxidative and nutrient stresses, the upregulation of autophagy can also mediate resistance to chemotherapy and radiation therapy. For instance, inhibiting autophagy with chloroquine enhanced the therapeutic efficacy of both the chemotherapy drugs oxiplatin and gemcitabine in an orthotopic murine model of pancreatic cancer (Loux *et al.,* 2010). Importantly, the mechanisms that underpin the upregulation of autophagy across various cancers remain to be elucidated.

An accumulating body of evidence suggests that oxidative stress regulates the autophagy pathway (McClung *et al.,* 2010; Nezis and Stenmark, 2012; Filomeni, Zio and Cecconi, 2014). The present work demonstrated that two cell stress treatments, 20 min H_2O_2 treatment and 48 h nutrient starvation, were capable of stimulating autophagy in OE19 cells, as demonstrated by the significantly increased number of autophagosomes and significantly reduced levels of SQSTM1 (Fig. 10; Fig. 13). An increased number of autophagosomes determined by immunofluorescence and reduced levels of SQSTM1 assessed by Western blotting are routinely used as two reliable methods of determining autophagy induction in cells (Bjørkøy *et al.,* 2009; Carroll *et al.,* 2018). Furthermore, an increased number of LC3-labelled autophagosomes can be seen following 20 and 30 min H_2O_2 treatment, supporting the notion that H_2O_2-induced stress promotes autophagy (Fig. 19). The autophagosome is the hallmark of macroautophagy (Mijaljica, Prescott and Devenish, 2012), and thus the present study focuses solely on stimulating the macroautophagic process (referred to here as simply autophagy). The LC3-II/LC3-I ratio, determined by Western blotting, is also indicative of the formation of autophagosomes and could have been used to further demonstrate autophagy induction in the present study.

Both H_2O_2 and nutrient stress treatments are capable of generating oxidative stress. The Fenton's reaction between H_2O_2 and Fe^{2+} ions generates the highly damaging hydroxyl radical, which is thought to be a major source of oxidative damage (Ward *et al.,* 1987). In contrast, nutrient starvation can cause metabolic stress and a higher demand for ATP, leading to mitochondrial overburden and electron leakage that ultimately triggers

excessive generation of reactive oxygen species (Ophuis *et al.,* 2009; Taucher *et al.,* 2022). Nutrient starvation is also known to induce autophagy through the involvement of PI3K/AMPK and other nutrient-sensing pathways (Alers *et al.,* 2012; Chiao *et al.,* 2013). The present findings thus support the notion that nutrient and oxidative stress stimulates the autophagy pathway.

Intriguingly, the levels of AGR2 significantly increased in OE19 cells during 20 min H_2O_2 treatment and 48 h nutrient starvation, compared to controls (Fig. 14). The increase in AGR2 levels appeared to be due to enhanced autophagy stimulation as treating cells with chloroquine reduced the levels of AGR2, compared to the relevant cell stress treatment without chloroquine (Fig. 14). The decrease in SQSTM1 levels was cancelled out by chloroquine, suggesting that chloroquine treatment did indeed inhibit autophagy (Fig. 13). The short 20 min time frame in which AGR2 levels significantly increased during H_2O_2 treatment suggests a potential reduction in the proteolytic degradation of AGR2, possibly as part of a pro-survival autophagy response to oxidative stress conditions. Overall, these findings provide further insights into the complex relationship between cellular stress, autophagy, and cancer, and suggest that AGR2 may be an important player in these processes (Fig. 4).

The AGR2 expressing OE19 cells were more sensitive to chloroquine compared with the AGR2 non-expressing OE33 cells; the CC_{50} was determined as 56 μM and 103 μM in OE19 and OE33 cells, respectively (Fig. 22). Although many inter-tumour differences may underlie this variation in autophagy inhibition sensitivity, this finding supports future knockout studies exploring the potential oncogenic role of AGR2 in pro-survival autophagy. Experiments investigating any potential difference in chloroquine sensitivity between OE19 control cells and those with silenced AGR2 expression or harbouring mutations of its single cysteine (C81) could reveal further insights into the potential role of AGR2 in pro-survival autophagy. It would also be interesting to investigate any potential reduction in cell viability that may be induced by knocking out AGR2 (or introducing mutations of C81) during exposure of OE19 cells to oxidative stress treatment, compared to controls. Should knocking out AGR2 lead to an increased sensitivity to oxidative stress, repeating the experiment in AGR2 knockout cells and controls with or without concomitant chloroquine treatment would provide insight into the extent to which AGR2 may utilise autophagy to promote cellular survival.

Many studies have reported the anticancer potential of chloroquine when used as a monotherapy or in combination with chemotherapy across a range of different tumour

types (Joshi *et al.,* 2012; Maycotte *et al.,* 2015; Hu *et al.,* 2016; Eloranta *et al.,* 2020). However, the efficacy of chloroquine in cancers of the oesophagus has not previously been reported. The reduced viability of the OE19 and OE33 cell lines from concentrations of chloroquine in the micromolar range encourages further investigation into the potential therapeutic benefits of chloroquine for oesophageal adenocarcinoma (Fig. 22). Treatment with 30 μM chloroquine for 48 h increased the levels of SQSTM1 in the OE19 cells (Fig. 13), suggesting that the antiproliferative effects of chloroquine treatment could be due to its anti-autophagic effects. The finding that chloroquine had a greater cytotoxic effect on the OE19 cells, compared to the OE33 cells, also supports future studies using a biomarker-driven approach to select subpopulations of patients (based on tumour expression profiles) that are likely to receive the most benefit from chloroquine treatment. Both AGR2 and SQSTM1 exhibit frequent gene amplification in multiple tumours (Fig. 23); thus, it would be interesting to explore whether high levels of AGR2 or SQSTM1 correlate with improved patient responses to chloroquine treatment.

4.3. The interaction between AGR2 and SQSTM1 – a topological conundrum

The interaction between AGR2 and SQSTM1, verified in Figure 5, poses a topological issue. AGR2 normally resides in the endoplasmic reticulum, but can also be localised to the plasma membrane, extracellular matrix and nucleus in the cancer context (Fourtouna *et al.,* 2009; Gupta, Dong and Lowe, 2012; Fessart *et al.,* 2016). In contrast, SQSTM1 is primarily located in the cytosol within the autophagosomes and lysosomes (Berkamp, Mostafavi and Sachse, 2020). As expected, a punctate distribution of SQSTM1 marking the autophagosomes/lysosomes was observed in OE19 cells by immunofluorescence (Fig. 8). Under normal conditions, the majority of AGR2 colocalised with P4HB in the endoplasmic reticulum (Fig. 6), which corresponded with previous findings (Worfolk *et al.,* 2019). Although there was not clear colocalization between AGR2 and SQSTM1, some areas of overlap were visible (Fig. 8). It is worthy to note that the small size and roundness of the OE19 cells made precisely determining the cellular localisation of AGR2 difficult during this study.

An increasing aggregation-promoting effect on AGR2 was observed during increasing periods of oxidative stress induced by H_2O_2 treatment (Fig. 17). These AGR2 aggregates appeared similar in shape (roughly circular) and size (~0.5 μm) to suggest they may be present within autophagosomes. However, AGR2 aggregates showed no colocalization with the autophagosome marker LC3, and thus the aggregation of AGR2 is unlikely to be due to its inclusion within autophagosomes (Fig. 19). Therefore, other factors are likely

to account for the observed aggregation of AGR2, including perhaps its enclosure in vesicles or an association with mucin complexes. Many of these AGR2 aggregates present during H_2O_2 treatment were observed in close proximity to the plasma membrane (Fig. 17). There was also evidence that AGR2 localised closer towards the plasma membrane during 48 h nutrient deprivation, compared to untreated controls (Fig. 15). It is therefore interesting to speculate whether AGR2 may remain associated with mucin granules following their export from the endoplasmic reticulum. During mucin secretion, post-Golgi vesicles containing mature polymeric mucins undergo lateral fusion to form the mucin granules, which are then exocytosed at a regulated rate to ensure the appropriate secretion of mucins (Adler, Tuvim and Dickey, 2013). The presence of AGR2 at the mucin granule may explain its aggregation near the plasma membrane (Fig. 9; Fig. 17), and potentially provide a mechanism by which AGR2 is secreted from oesophageal adenocarcinoma cells (Fig. 20).

The presence of AGR2 at the mucin granule may also explain the topological conundrum regarding its interaction with SQSTM1. A recent study demonstrated that the autophagy pathway plays a role in removing excess non-secreted intracellular mucin granules during the resolution of a state of airway inflammation termed mucous metaplasia (Sweeter *et al.,* 2021). Sweeter *et al.* showed that stimulation of autophagy via mTOR inhibition resulted in a reduction in the levels of MUC5AC in human airway epithelial cells. Furthermore, they used immunostaining and structured illumination microscopy to demonstrate that LC3 and Lamp1 labelled autolysosomes come into close contact with, and subsequently engulf, mucin granules. It is possible that this autophagy response to remove excess mucin granules during inflammatory insult in oesophageal glandular cells may also occur in oesophageal adenocarcinoma, in which inflammation is key in driving tumour development (O'Sullivan *et al.,* 2014). In such a theory, it is possible to envision that SQSTM1 at the autophagosome would closely approximate AGR2 at the mucin granule to enable the AGR2-SQSTM1 interaction to take place. Further investigation into the precise localisation of AGR2, SQSTM1 and mucins in OE19 cells, under both control and cell stress conditions, is required to explore such a theory.

Given that AGR2 is secreted from oesophageal adenocarcinoma cells (Fig. 20), another possibility is that AGR2 could be endocytosed from the extracellular environment into the cell to then be degraded by selective autophagy mediated by SQSTM1. Such a mechanism would therefore permit the close association between AGR2 and SQSTM1 to enable their interaction. This theory would also be in accordance with the observed aggregation of

AGR2 (perhaps enclosed in vesicles) in close proximity to the plasma membrane (Fig. 15; Fig. 17). The interaction between AGR2 and SQSTM1 has thus far only been identified in oesophageal adenocarcinoma (Worfolk *et al.,* 2019), and is likely to be the result of perturbed oncogenic signalling. However, further work is required to establish whether AGR2 also interacts with SQSTM1 in non-malignant cells.

It is worthy to note that the AGR2-SQSTM1 interaction, identified by immunoprecipitation followed by Western blotting (Fig. 7), could in fact occur artefactually during post-lysis oxidation reactions. This notion would potentially explain the topological issue regarding the AGR2-SQSTM1 interaction and the limited colocalization observed between AGR2 and SQSTM1 in immunofluorescence experiments (Fig. 8 and 9). Wofolk *et al.* (2019) lysed OE19 cells in the presence or absence of NEM, an alkylating agent that blocks sulphydryl groups to prevent disulphide bond formation. The authors then used immunoprecipitation followed by mass spectrometry and SQSTM1 was identified as an AGR2 interacting protein that was detected only when cells were lysed in the absence of NEM. It was concluded that the AGR2-SQSTM1 association could not be observed in the presence of NEM because this strong alkylating agent would disrupt the disulphide bonds in this interaction. However, pre-treatment of cells with alkylating agents is an important procedure utilised to reduce post-lysis oxidation reactions, bringing the validity of the AGR2-SQSTM1 interaction into question. Worfolk *et al.* (2019) also lysed adenocarcinoma tissue in the presence or absence of NEM and used AGR2 immunoprecipitation followed by Western blotting to detect MUC-5AC. Importantly, the interaction between AGR2 and the lower molecular weight forms of mucin were also only visible in the absence of NEM. The disulphide-dependent interactions between AGR2 and the mucins MUC1, MUC2 and MUC-5AC to enable their correct folding and secretion are well established (Park *et al.,* 2009; Schroeder *et al.,* 2012; Norris *et al.,* 2013). Therefore, it would appear that NEM is likely to interfere with the ability of AGR2 to form disulphide-dependent interactions with its client proteins.

4.4. How is AGR2 secreted from oesophageal adenocarcinoma cells?

AGR2 normally resides in the endoplasmic reticulum to perform its protein folding functions (Gupta, Dong and Lowe, 2012). However, the secretion of AGR2 into the extracellular environment has been reported in various different cancer types, which are summarised in Table 1. The present study is believed to be the first to describe the secretion of AGR2 from oesophageal adenocarcinoma cells (Fig. 20). Proteins that are

secreted into the extracellular environment collectively form an important class of proteins referred to as the secretome (Tjalsma *et al.,* 2004). Tumour secretomes often exhibit altered compositions compared to the normal tissues from which they were derived and they can play a functional role in promoting tumorigenesis (Peinado, Lavotshkin and Lyden, 2011; Valerie, Weaver and Werb, 2012). An accumulating body of research discussed previously has shed some light on the functions of extracellular AGR2, including its implications in the promotion of metastasis, proliferation, angiogenesis and inflammation (Fig. 3). However, the function of extracellular AGR2 in oesophageal cancers does not appear to have been previously investigated.

Because oesophageal adenocarcinoma is a key example of an inflammation driven cancer (O'Sullivan *et al.,* 2014), it seems rational to investigate a potential pro-inflammatory role for AGR2 in the extracellular environment of this cancer. Intriguingly, the link between AGR2 and inflammation has previously been reported in inflammatory bowel disease, in which AGR2 secretion upon endoplasmic reticulum stress was reported to mediate pro-inflammatory responses (Maurel *et al.,* 2019). To investigate the link between AGR2 and inflammation, Maurel *et al.* exposed peripheral blood mononuclear cells from three healthy human volunteers to media conditioned by cells ectopically overexpressing AGR2. In the extracellular milieu, AGR2 was found to play a direct role in the chemoattraction of monocytes from peripheral blood mononuclear cells. Monocyte migration was disrupted by AGR2 blocking antibodies. Therefore, it is plausible that AGR2 performs an oncogenic role as a pro-inflammatory chemokine in the tumour secretome.

Table 1. The secretion of AGR2 reported across different cancers

Cancer type	Cell model	Reference
Breast	MCF-7, RAMA 37 and T47D	Clarke, Rudland and Barraclough, 2015; Li *et al.,* 2016
Prostate	PCa, PC3, PC3M-Luc, RWPE-1, HUCECs, LuCaP and 22Rv1	Vitello *et al.,* 2016; Garri *et al.,* 2018; Jia *et al.,* 2018; Tiemann *et al.,* 2019
Pancreatic	SU.86.86 and MPanc-96	Ramachandran *et al.,* 2008
Colorectal	HT29	Tian *et al.,* 2018
Glioblastoma	UA87 and LN18	Hong, Wang and Li, 2013
Lung adenocarcinoma	H23	Fessart *et al.,* 2016

Many secretory proteins utilise the conventional secretory pathway that passes through the endoplasmic reticulum and Golgi before reaching the plasma membrane. Proteins designated for secretion by this conventional pathway possess a N-terminal signal sequence. The signal sequence will usually be cleaved off by an extracellular signal peptidase following exocytosis (Jackson and Blobel, 1977). Most signal sequences will consist of three distinct domains: a positively charged n-region, a hydrophobic h-region, and a polar c-region containing the cleavage site (Choo, Tan and Ranganathan, 2005). However, secretory proteins show a high degree of variation in signal sequence conservation and length (Hiller *et al.,* 2004). Many secretory proteins exist in human cells that do not use the classical endoplasmic reticulum-Golgi pathway, and instead are secreted through unconventional secretory pathways (Kim, Gee and Lee, 2018). In human cells, unconventional protein secretion includes translocation across the plasma membrane via pores (Zacherl *et al.,* 2015); export by ATP-binding cassette (ABC) transporters (McGrath and Varshavsky, 1989); secretion of transmembrane proteins that omit the Golgi in an otherwise conventional route (Gee *et al.,* 2011); and autophagy-associated secretion via autophagosomes (Duran *et al.,* 2010).

Using PrediSi, a predicted signal peptide from Met1-Ala20 was identified in the N-terminus of AGR2 with 96% confidence, indicating that AGR2 is likely to follow the conventional secretory pathway (Fig. 21). This signal sequence may be conserved from the *Xenopus* orthologue of AGR2 known as XAG-2, which is secreted to induce cement gland differentiation (Aberger *et al.,* 1998). Furthermore, unconventional protein secretion pathways are stimulated in human cells by nutrient starvation and other stressors (Cruz-Garcia *et al.,* 2014; Kim, Gee and Lee, 2018). No increased secretion of AGR2 from OE19 cells was observed during nutrient starvation or H_2O_2-stressed conditions (Fig. 20), further supporting the notion that AGR2 is not secreted via unconventional pathways. It would also be possible to label AGR2 with Green Fluorescent Protein (GFP) and use live cell microscopy to visualise protein progression through the secretory pathway as demonstrated previously (Presley *et al.,* 1997).

Furthermore, it has been demonstrated that AGR2 is *O*-glycosylated upon secretion in human and rat cell lines (Clarke, Rudland and Barraclough, 2015). Most secreted proteins are glycosylated in the Golgi apparatus (Bosques, Raguram and Sasisekharan, 2006). Therefore, this is further evidence to indicate that AGR2 passes through the Golgi apparatus as part of the conventional secretory pathway. Aberrant glycosylation, in particular increased *O*-glycosylation of proteins, is a hallmark of cancerous cells (Wang

et al., 2020). These findings indicate a potential function for *O*-glycosylation in the secretion of AGR2 from cancerous cells. It would be intriguing to mutate this glycosylation site (currently undetermined) in AGR2 to investigate the functional consequences of glycosylation on AGR2 secretion and the previously reported oncogenic activities of extracellular AGR2, such as inflammation, metastasis and angiogenesis (Fig. 3).

Another motif associated with the secretion of AGR2 is the endoplasmic reticulum retrieval sequence KTEL, which is located at the C-terminus (Fig. 2). The classical endoplasmic reticulum retrieval motif is the KDEL, although variants such as the KTEL motif are known to similarly retrieve proteins to the endoplasmic reticulum with a reduced affinity for the KDEL receptor (Raykhel *et al.,* 2007; Alanen *et al.,* 2011). It is tempting to speculate that the non-canonical KTEL motif may lower the affinity of AGR2 to the KDEL receptor, enabling the diverse trafficking of this protein when overexpressed in cancer. However, HEK-293T cells transfected with AGR2 constructs in which the KTEL motif was mutated to either a KDEL or a STOP were shown to secrete similar levels of AGR2 to that observed in cells expressing wild-type AGR2 (Fessart *et al.,* 2016). HEK-293T cells do not express AGR2 endogenously, and thus it would be interesting to investigate how mutation of the KTEL to either a KDEL or a STOP may alter the secretion of endogenously expressed AGR2 in the OE19 cells. CRISPR screening, in which single guide RNAs could target specific amino acids in AGR2, would be useful to outline domains involved in the secretion of AGR2 into OE19 culture media. Motifs of particular interest in AGR2 secretion include the predicted signal sequence, the KTEL, and the dimerization motif at the thioredoxin-like domain (CPHS).

4.5. Conclusions and future outlooks

The present work demonstrates that endogenous AGR2 can form disulphide dependent complexes in OE19 cells through its single cysteine residue in its thioredoxin-like domain (Fig. 5). Because AGR2 lacks dual cysteines with full redox capacity, the mechanism by which it mediates disulphide bond formation with SQSTM1 or its mucin clients remains unclear. Three possible solutions to this conundrum include: firstly, dimeric AGR2 provides full redox capacity to permit disulphide bond formation; secondly, additional redox enzymes assist AGR2 to perform full redox reactions; or, lastly, the single cysteine residue in AGR2 enables the isomerisation (rearrangement) of crucial disulphide bonds in its protein clients.

AGR2 interacts with the autophagy receptor SQSTM1 (Fig. 7), an interaction which was previously shown to be mediated by disulphide bonds (Worfolk *et al.,* 2019). Disulphide bond formation is known to be required in SQSTM1 to stimulate pro-survival autophagy (Carroll *et al.,* 2018), and thus it is plausible that AGR2 may be involved in the oxidation of SQSTM1. Therefore, it was hypothesised that the upregulation of AGR2 and SQSTM1 across various cancers could be involved in the induction of autophagy to promote cellular survival under the high levels of oxidative stress that cancerous cells are exposed to (Fig. 4). Levels of AGR2 significantly increased in OE19 cells during autophagy stimulation induced by H_2O_2 treatment and nutrient starvation, which further links AGR2 with autophagy responses to oxidative stress (Fig. 13; Fig. 14).

Carroll *et al.* (2018) reported that mouse embryonic fibroblasts lacking SQSTM1 or expressing the C105A,C113A mutant were more susceptible to cell death when exposed to oxidative stress than those cells expressing wild type SQSTM1. Treatment with chloroquine cancelled out this difference in cell survival between the cells expressing wild type SQSTM1 and those lacking SQSTM1 or expressing the C105A,C113A mutant, highlighting autophagy as the pro-survival mechanism. It would be interesting to investigate whether cells with silenced AGR2 or expressing AGR2 mutants lacking the C81 residue would also be more susceptible to oxidative stress, compared to those expressing wild-type AGR2. If AGR2 was indeed responsible for the oxidation of SQSTM1 required to stimulate pro-survival autophagy, it would be expected that cells expressing a C81A mutant of AGR2 would have a higher percentage of cell death during oxidative stress to those expressing wild-type AGR2. Indeed, the cells expressing the C81 mutant of AGR2 would be expected to show a similar percentage of cell death during oxidative stress to cells expressing the C105A,C113A mutant of SQSTM1. Furthermore, it would be expected that chloroquine would cancel out the difference in cell survival between cells expressing the C81 mutant of AGR2 and cells expressing wild-type AGR2 and SQSTM1, identifying autophagy as the resistance mechanism.

Chloroquine reduced the viability of OE19 and OE33 cell lines in a dose-dependent manner (Fig. 22), encouraging further investigation into the potential therapeutic benefits of autophagy inhibition as a monotherapy or in combination strategies for oesophageal adenocarcinoma. Chemotherapy and radiation therapy are treatments used for oesophageal adenocarcinoma that generate oxidative stress to induce cell death, although various mechanisms to ameliorate oxidative stress in cancerous cells can lead to drug resistance (Chen *et al.,* 2021). Evidence in the present work suggests there may be a

rationale for combining AGR2 inhibitors or chloroquine with chemotherapy or radiation therapy to overcome resistance associated with autophagy upregulation to promote cellular survival during oxidative stress.

The interaction between AGR2 and SQSTM1 poses a topological conundrum. As expected, a punctate distribution of SQSTM1 marking the autophagosomes was observed in OE19 cells by immunofluorescence (Fig. 8). However, the majority of AGR2 localised at the endoplasmic reticulum (Fig. 6), which corresponded with previous findings (Worfolk *et al.,* 2019). During oxidative stress conditions, AGR2 formed aggregates in close proximity to the plasma membrane (Fig. 17). AGR2 aggregates showed no colocalization with the autophagosome marker LC3, and thus the aggregation of AGR2 is unlikely to be due to its inclusion within autophagosomes (Fig. 19). The presence of AGR2 aggregates in close proximity to the plasma membrane may be explained by a possible association of AGR2 with mucin granules. It is possible that SQSTM1-mediated selective autophagy may be involved in the removal of AGR2-associated mucin granules, perhaps bringing AGR2 and SQSTM1 in proximity for their interaction.

The present work is believed to be the first to report the secretion of AGR2 from oesophageal adenocarcinoma cells (Fig. 20). Furthermore, a predicted signal peptide was identified in the N-terminus of AGR2 (Fig. 21). It is thus plausible that AGR2 may follow the conventional secretory pathway along the endoplasmic reticulum-Golgi-plasma membrane route that mucin granules also follow during their processing and secretion (Adler, Tuvim and Dickey, 2013). The presence of AGR2 in the extracellular milieu has been implicated with numerous oncogenic functions discussed previously, including inflammation, angiogenesis, metastasis and proliferation (Fig. 3). Further work is required to elucidate the precise mechanisms by which secreted AGR2 may mediate such functions, particularly with regard to oesophageal cancers which have been comparatively understudied.

In sum, AGR2 appears to function at the core of a perplexing relationship between mucin processing, autophagy, and cancer. Elucidating the mechanisms bridging AGR2 and the aforementioned functions may provide a holistic understanding of its oncogenic role and create novel therapeutic strategies.

References

Aberger, F., Weidinger, G., Grunz, H. and Richter, K., 1998. Anterior specification of embryonic ectoderm: the role of the Xenopus cement gland-specific gene XAG-2. *Mechanisms of development*, *72*(1-2), pp.115-130.

Adams, O., Dislich, B., Berezowska, S., Schläfli, A.M., Seiler, C.A., Kroell, D., Tschan, M.P. and Langer, R., 2016. Prognostic relevance of autophagy markers LC3B and p62 in esophageal adenocarcinomas. *Oncotarget*, *7*(26), p.39241.

Adams, B.M., Oster, M.E. and Hebert, D.N., 2019. Protein quality control in the endoplasmic reticulum. *The protein journal*, *38*(3), pp.317-329.

Adler, K.B., Tuvim, M.J. and Dickey, B.F., 2013. Regulated mucin secretion from airway epithelial cells. *Frontiers in endocrinology*, *4*(129), p.129.

Alanen, H.I., Raykhel, I.B., Luukas, M.J., Salo, K.E. and Ruddock, L.W., 2011. Beyond KDEL: the role of positions 5 and 6 in determining ER localization. *Journal of molecular biology*, *409*(3), pp.291-297.

Alers, S., Löffler, A.S., Wesselborg, S. and Stork, B., 2012. Role of AMPK-mTOR-Ulk1/2 in the regulation of autophagy: cross talk, shortcuts, and feedbacks. *Molecular and cellular biology*, *32*(1), pp.2-11.

Araki, K. and Inaba, K., 2012. Structure, mechanism, and evolution of Ero1 family enzymes. *Antioxidants & redox signaling*, *16*(8), pp.790-799.

Arfin, S., Jha, N.K., Jha, S.K., Kesari, K.K., Ruokolainen, J., Roychoudhury, S., Rathi, B. and Kumar, D., 2021. Oxidative stress in cancer cell metabolism. *Antioxidants, 10*(5), p.642.

Arumugam, T., Deng, D., Bover, L., Wang, H., Logsdon, C.D. and Ramachandran, V., 2015. New blocking antibodies against novel AGR2–C4. 4A pathway reduce growth and metastasis of pancreatic tumors and increase survival in mice. *Molecular cancer therapeutics*, *14*(4), pp.941-951.

Barraclough, D.L., Platt-Higgins, A., de Silva Rudland, S., Barraclough, R., Winstanley, J., West, C.R. and Rudland, P.S., 2009. The metastasis-associated anterior gradient 2 protein is correlated with poor survival of breast cancer patients. *The American journal of pathology*, *175*(5), pp.1848-1857.

Benham, A.M., 2012. The protein disulfide isomerase family: key players in health and disease. *Antioxidants & redox signaling*, *16*(8), pp.781-789.

Benham, A.M., 2019. Endoplasmic Reticulum redox pathways: In sickness and in health. *The FEBS journal*, *286*(2), pp.311-321.

Bennett, E.P., Mandel, U., Clausen, H., Gerken, T.A., Fritz, T.A. and Tabak, L.A., 2012. Control of mucin-type O-glycosylation: a classification of the polypeptide GalNAc-transferase gene family. *Glycobiology*, *22*(6), pp.736-756.

Berkamp, S., Mostafavi, S. and Sachse, C., 2021. Structure and function of p62/SQSTM1 in the emerging framework of phase separation. *The FEBS journal*, *288*(24), pp.6927-6941.

Bjørkøy, G., Lamark, T., Pankiv, S., Øvervatn, A., Brech, A. and Johansen, T., 2009. Monitoring autophagic degradation of p62/SQSTM1. *Methods in enzymology*, *452*, pp.181-197.

Braakman, I., Helenius, J. and Helenius, A., 1992. Manipulating disulfide bond formation and protein folding in the endoplasmic reticulum. *The EMBO journal*, *11*(5), pp.1717-1722.

Brychtova, V., Vojtesek, B. and Hrstka, R., 2011. Anterior gradient 2: a novel player in tumor cell biology. *Cancer letters*, *304*(1), pp.1-7.

Carroll, B., Otten, E.G., Manni, D., Stefanatos, R., Menzies, F.M., Smith, G.R., Jurk, D., Kenneth, N., Wilkinson, S., Passos, J.F. and Attems, J., 2018. Oxidation of SQSTM1/p62 mediates the link between redox state and protein homeostasis. *Nature communications*, *9*(1), pp.1-11.

Chen, Y., Li, Y., Huang, L., Du, Y., Gan, F., Li, Y. and Yao, Y., 2021. Antioxidative stress: inhibiting reactive oxygen species production as a cause of radioresistance and chemoresistance. *Oxidative Medicine and Cellular Longevity*, *21*, pp.1-16.

Chevet, E., Fessart, D., Delom, F., Mulot, A., Vojtesek, B., Hrstka, R., Murray, E., Gray, T. and Hupp, T., 2013. Emerging roles for the pro-oncogenic anterior gradient-2 in cancer development. *Oncogene*, *32*(20), pp.2499-2509.

Chiao, M.T., Cheng, W.Y., Yang, Y.C., Shen, C.C. and Ko, J.L., 2013. Suberoylanilide hydroxamic acid (SAHA) causes tumor growth slowdown and triggers autophagy in glioblastoma stem cells. *Autophagy*, *9*(10), pp.1509-1526.

Ciriello, G. and Magnani, L., 2021. The many faces of cancer evolution. *Iscience, 24*(5).

Choo, K.H., Tan, T.W. and Ranganathan, S., 2005. SPdb–a signal peptide database. *BMC bioinformatics*, *6*(1), pp.1-8.

Chude, C.I. and Amaravadi, R.K., 2017. Targeting autophagy in cancer: update on clinical trials and novel inhibitors. *International journal of molecular sciences*, *18*(6), p.1279

Clarke, C., Rudland, P. and Barraclough, R., 2015. The metastasis-inducing protein AGR2 is O-glycosylated upon secretion from mammary epithelial cells. *Molecular and cellular biochemistry*, *408*(1), pp.245-252.

Curran, D.R. and Cohn, L., 2010. Advances in mucous cell metaplasia: a plug for mucus as a therapeutic focus in chronic airway disease. *American journal of respiratory cell and molecular biology*, *42*(3), pp.268-275.

Davis, C.W. and Dickey, B.F., 2008. Regulated airway goblet cell mucin secretion. *Annu. rev. physiol*, *70*, pp.487-512.

Desideri, E., Filomeni, G. and Ciriolo, M.R., 2012. Glutathione participates in the modulation of starvation-induced autophagy in carcinoma cells. *Autophagy*, *8*(12), pp.1769-1781.

Dice, J.F., 1990. Peptide sequences that target cytosolic proteins for lysosomal proteolysis. *Trends in biochemical sciences*, *15*(8), pp.305-309.

Dumartin, L., Alrawashdeh, W., Trabulo, S.M., Radon, T.P., Steiger, K., Feakins, R.M., Di Magliano, M.P., Heeschen, C., Esposito, I., Lemoine, N.R. and Crnogorac-Jurcevic, T., 2017. ER stress protein AGR2 precedes and is involved in the regulation of pancreatic cancer initiation. *Oncogene*, *36*(22), pp.3094-3103.

Duran, J.M., Anjard, C., Stefan, C., Loomis, W.F. and Malhotra, V., 2010. Unconventional secretion of Acb1 is mediated by autophagosomes. *Journal of cell biology*, *188*(4), pp.527-536.

Ellgaard, L. and Ruddock, L.W., 2005. The human protein disulphide isomerase family: substrate interactions and functional properties. *EMBO reports, 6*(1), pp.28-32.

Eloranta, K., Cairo, S., Liljeström, E., Soini, T., Kyrönlahti, A., Judde, J.G., Wilson, D.B., Heikinheimo, M. and Pihlajoki, M., 2020. Chloroquine triggers cell death and inhibits PARPs in cell models of aggressive hepatoblastoma. *Frontiers in oncology*, *10*, p.1138.

Fessart, D., Domblides, C., Avril, T., Eriksson, L.A., Begueret, H., Pineau, R., Malrieux, C., Dugot-Senant, N., Lucchesi, C., Chevet, E. and Delom, F., 2016. Secretion of protein disulphide isomerase AGR2 confers tumorigenic properties. *Elife*, *5*, p.13887.

Fletcher, G.C., Patel, S., Tyson, K., Adam, P.J., Schenker, M., Loader, J.A., Daviet, L., Legrain, P., Parekh, R., Harris, A.L. and Terrett, J.A., 2003. hAG-2 and hAG-3, human homologues of genes involved in differentiation, are associated with oestrogen receptor-positive breast tumours and interact with metastasis gene C4. 4a and dystroglycan. *British journal of cancer*, *88*(4), pp.579-585.

Filomeni, G., De Zio, D. and Cecconi, F., 2015. Oxidative stress and autophagy: the clash between damage and metabolic needs. *Cell death & differentiation*, *22*(3), pp.377-388.

Fourtouna, A., Murray, E., Nicholson, J., Maslon, M.M., Pang, L.Y., Dryden, D.T. and Hupp, T.R., 2009. The anterior gradient-2 pathway as a model for developing peptide-aptamer anti-cancer drug leads that stimulate p53 function. *Current chemical biology*, *3*(2), pp.124-137.

Galligan, J.J. and Petersen, D.R., 2012. The human protein disulfide isomerase gene family. *Human genomics*, *6*(6), pp.1-15.

Garri, C., Howell, S., Tiemann, K., Tiffany, A., Jalali-Yazdi, F., Alba, M.M., Katz, J.E., Takahashi, T.T., Landgraf, R., Gross, M.E. and Roberts, R.W., 2018. Identification, characterization and application of a new peptide against anterior gradient homolog 2 (AGR2). *Oncotarget*, *9*(44), p.27363.

Gee, H.Y., Noh, S.H., Tang, B.L., Kim, K.H. and Lee, M.G., 2011. Rescue of ΔF508-CFTR trafficking via a GRASP-dependent unconventional secretion pathway. *Cell*, *146*(5), pp.746-760.

Glick, D., Barth, S. and Macleod, K.F., 2010. Autophagy: cellular and molecular mechanisms. *The Journal of pathology, 221*(1), pp.3-12.

Guo, H., Chen, H., Zhu, Q., Yu, X., Rong, R., Merugu, S.B., Mangukiya, H.B. and Li, D., 2016. A humanized monoclonal antibody targeting secreted anterior gradient 2 effectively inhibits the xenograft tumor growth. *Biochemical and biophysical research communications*, *475*(1), pp.57-63.

Guo, H., Zhu, Q., Yu, X., Merugu, S.B., Mangukiya, H.B., Smith, N., Li, Z., Zhang, B., Negi, H., Rong, R. and Cheng, K., 2017. Tumor-secreted anterior gradient-2 binds to VEGF and FGF2 and enhances their activities by promoting their homodimerization. *Oncogene, 36*, pp.5098-5109.

Gupta, A., Dong, A. and Lowe, A.W., 2012. AGR2 gene function requires a unique endoplasmic reticulum localization motif. *Journal of biological chemistry*, *287*(7), pp.4773-4782.

Hao, C., Liu, G. and Tian, G., 2019. Autophagy inhibition of cancer stem cells promotes the efficacy of cisplatin against non-small cell lung carcinoma. *Therapeutic advances in respiratory disease*, *13*, pp.1-11.

He, L., Zhang, J., Zhao, J., Ma, N., Kim, S.W., Qiao, S. and Ma, X., 2018. Autophagy: the last defence against cellular nutritional stress. *Advances in nutrition*, *9*(4), pp.493-504.

Higa, A., Mulot, A., Delom, F., Bouchecareilh, M., Nguyên, D.T., Boismenu, D., Wise, M.J. and Chevet, E., 2011. Role of pro-oncogenic protein disulfide isomerase (PDI) family member anterior gradient 2 (AGR2) in the control of endoplasmic reticulum homeostasis. *Journal of biological chemistry*, *286*(52), pp.44855-44868.

Hiller, K., Grote, A., Scheer, M., Münch, R. and Jahn, D., 2004. PrediSi: prediction of signal peptides and their cleavage positions. *Nucleic acids research*, *32*(2), pp.375-379.

Hong, X.Y., Wang, J. and Li, Z., 2013. AGR2 expression is regulated by HIF-1 and contributes to growth and angiogenesis of glioblastoma. *Cell biochemistry and biophysics*, *67*, pp.1487-1495.

Hrstka, R., Bouchalova, P., Michalova, E., Matoulkova, E., Muller, P., Coates, P.J. and Vojtesek, B., 2016. AGR2 oncoprotein inhibits p38 MAPK and p53 activation through a DUSP10-mediated regulatory pathway. *Molecular oncology*, *10*(5), pp.652-662.

Hrstka, R., Nenutil, R., Fourtouna, A., Maslon, M.M., Naughton, C., Langdon, S., Murray, E., Larionov, A., Petráková, K., Muller, P. and Dixon, M.J., 2010. The pro-metastatic protein anterior gradient-2 predicts poor prognosis in tamoxifen-treated breast cancers. *Oncogene*, *29*(34), pp.4838-4847.

Hu, T., Li, P., Luo, Z., Chen, X., Zhang, J., Wang, C., Chen, P. and Dong, Z., 2016. Chloroquine inhibits hepatocellular carcinoma cell growth in vitro and in vivo. *Oncology reports*, *35*(1), pp.43-49.

Jackson, R.C. and Blobel, G., 1977. Post-translational cleavage of presecretory proteins with an extract of rough microsomes from dog pancreas containing signal peptidase activity. *Proceedings of the national academy of sciences*, *74*(12), pp.5598-5602.

Jakobi, A.J., Huber, S.T., Mortensen, S.A., Schultz, S.W., Palara, A., Kuhm, T., Shrestha, B.K., Lamark, T., Hagen, W.J., Wilmanns, M. and Johansen, T., 2020. Structural basis of p62/SQSTM1 helical filaments and their role in cellular cargo uptake. *Nature communications*, *11*(1), p.440.

Jia, M., Guo, Y., Zhu, D., Zhang, N., Li, L., Jiang, J., Dong, Y., Xu, Q., Zhang, X., Wang, M. and Yu, H., 2018. Pro-metastatic activity of AGR2 interrupts angiogenesis target bevacizumab efficiency via direct interaction with VEGFA and activation of NF-κB pathway. *Biochimica et biophysica acta – molecular basis of disease*, *1864*(5), pp.1622-1633.

Joshi, P., Chakraborti, S., Ramirez-Vick, J.E., Ansari, Z.A., Shanker, V., Chakrabarti, P. and Singh, S.P., 2012. The anticancer activity of chloroquine-gold nanoparticles against MCF-7 breast cancer cells. *Colloids and surfaces B: biointerfaces*, *95*, pp.195-200.

Ju, L.L., Zhao, C.Y., Ye, K.F., Yang, H. and Zhang, J., 2016. Expression and clinical implication of Beclin1, HMGB1, p62, survivin, BRCA1 and ERCC1 in epithelial ovarian tumor tissues. *Eur rev med pharmacol sci*, *20*(10), pp.1993-2003.

Kalid, O., Gotliv, I., Levy-Apter, E., Beker, D.F., Cherniavsky-Lev, M., Rotem, E. and Miron, N., 2022. PTX80, A novel compound targeting the autophagy receptor p62/SQSTM1 for treatment of cancer. *Chemical biology & drug design, 100*(5), pp.623-638.

Kesimer, M., Makhov, A.M., Griffith, J.D., Verdugo, P. and Sheehan, J.K., 2010. Unpacking a gel-forming mucin: a view of MUC5B organization after granular release. *American journal of physiology-lung cellular and molecular physiology*, *298*(1), pp.15-22.

Kim, J., Gee, H.Y. and Lee, M.G., 2018. Unconventional protein secretion–new insights into the pathogenesis and therapeutic targets of human diseases. *Journal of cell science*, *131*(12), pp.1-11.

Kim, V., Kelemen, S.E., Abuel-Haija, M., Gaughan, J.P., Sharafkaneh, A., Evans, C.M., Dickey, B.F., Solomides, C.C., Rogers, T.J. and Criner, G.J., 2008. Small airway mucous metaplasia and inflammation in chronic obstructive pulmonary disease. *COPD: Journal of chronic obstructive pulmonary disease*, *5*(6), pp.329-338.

Kitamura, H., Torigoe, T., Asanuma, H., Hisasue, S.I., Suzuki, K., Tsukamoto, T., Satoh, M. and Sato, N., 2006. Cytosolic overexpression of p62 sequestosome 1 in neoplastic prostate tissue. *Histopathology*, *48*(2), pp.157-161.

Klis, F.M., Ram, A.F.J., Montijn, R.C., Kapteyn, J.C., Caro, L.H.P., Vossen, J.H., Van Berkel, M.A.A., Brekelmans, S.S.C. and Van den Ende, H., 1998. 13 posttranslational modifications of secretory proteins. *Methods in microbiology*, *26*, pp.223-238.

Kozlov, G., Määttänen, P., Thomas, D.Y. and Gehring, K., 2010. A structural overview of the PDI family of proteins. *The FEBS journal*, *277*(19), pp.3924-3936.

Lamark, T., Perander, M., Outzen, H., Kristiansen, K., Øvervatn, A., Michaelsen, E., Bjørkøy, G. and Johansen, T., 2003. Interaction codes within the family of mammalian Phox and Bem1p domain-containing proteins. *Journal of biological chemistry*, *278*(36), pp.34568-34581.

Li, X., He, S. and Ma, B., 2020. Autophagy and autophagy-related proteins in cancer. *Molecular cancer*, *19*(1), pp.1-16.

Li, Z., Zhu, Q., Chen, H., Hu, L., Negi, H., Zheng, Y., Ahmed, Y., Wu, Z. and Li, D., 2016. Binding of anterior gradient 2 and estrogen receptor-α: Dual critical roles in enhancing fulvestrant resistance and IGF-1-induced tumorigenesis of breast cancer. *Cancer letters*, *377*(1), pp.32-43.

Loux, T.J., Schapiro, N.E., Kang, R., Tang, D., Lotze, M.T. and Zeh, H.J., 2010. Inhibition of autophagy by chloroquine enhances chemotherapy in an orthotopic murine model of pancreatic cancer. *Journal of surgical research, 158*(2), pp.393-394.

Lu, P., Weaver, V.M. and Werb, Z., 2012. The extracellular matrix: a dynamic niche in cancer progression. *Journal of cell biology*, *196*(4), pp.395-406.

Ma, S.R., Wang, W.M., Huang, C.F., Zhang, W.F. and Sun, Z.J., 2015. Anterior gradient protein 2 expression in high grade head and neck squamous cell carcinoma correlated with cancer stem cell and epithelial mesenchymal transition. *Oncotarget*, *6*(11), p.8807.

Maurel, M., Obacz, J., Avril, T., Ding, Y.P., Papadodima, O., Treton, X., Daniel, F., Pilalis, E., Hörberg, J., Hou, W. and Beauchamp, M.C., 2019. Control of anterior gradient 2 (AGR2) dimerization links endoplasmic reticulum proteostasis to inflammation. *EMBO molecular medicine*, *11*(6), p.10120.

Mauthe, M., Orhon, I., Rocchi, C., Zhou, X., Luhr, M., Hijlkema, K.J., Coppes, R.P., Engedal, N., Mari, M. and Reggiori, F., 2018. Chloroquine inhibits autophagic flux by decreasing autophagosome-lysosome fusion. *Autophagy, 14*(8), pp.1435-1455.

Maycotte, P., Gearheart, C.M., Barnard, R., Aryal, S., Mulcahy Levy, J.M., Fosmire, S.P., Hansen, R.J., Morgan, M.J., Porter, C.C., Gustafson, D.L. and Thorburn, A., 2014. STAT3-mediated autophagy dependence identifies subtypes of breast cancer where autophagy inhibition can be efficaciousautophagy and STAT3 control breast cancer survival. *Cancer research*, *74*(9), pp.2579-2590.

McClung, J.M., Judge, A.R., Powers, S.K. and Yan, Z., 2010. p38 MAPK links oxidative stress to autophagy-related gene expression in cachectic muscle wasting. *American journal of physiology-cell physiology*, *298*(3), pp.542-549.

McGrath, J.P. and Varshavsky, A., 1989. The yeast STE6 gene encodes a homologue of the mammalian multidrug resistance P-glycoprotein. *Nature*, *340*(6232), pp.400-404.

Miesenböck, G. and Rothman, J.E., 1995. The capacity to retrieve escaped ER proteins extends to the trans-most cisterna of the Golgi stack. *The journal of cell biology, 129*(2), pp.309-319.

Mijaljica, D., Prescott, M. and Devenish, R.J., 2012. The intriguing life of autophagosomes. *International journal of molecular sciences, 13*(3), pp.3618-3635.

Mizushima, N. and Levine, B., 2010. Autophagy in mammalian development and differentiation. *Nature cell biology*, *12*(9), pp.823-830.

Mohamed, A., Ayman, A., Deniece, J., Wang, T., Kovach, C., Siddiqui, M.T. and Cohen, C., 2015. P62/Ubiquitin IHC expression correlated with clinicopathologic parameters and outcome in gastrointestinal carcinomas. *Frontiers in oncology*, *5*(70), pp.1-7.

Mohtar, M.A., Hernychova, L., O'Neill, J.R., Lawrence, M.L., Murray, E., Vojtesek, B. and Hupp, T.R., 2018. The sequence-specific peptide-binding activity of the protein sulfide isomerase AGR2 directs its stable binding to the oncogenic receptor EpCAM. *Molecular & cellular proteomics*, *17*(4), pp.737-763.

Moidu, N.A., Rahman, N.S.A., Syafruddin, S.E., Low, T.Y. and Mohtar, M.A., 2020. Secretion of pro-oncogenic AGR2 protein in cancer. *Heliyon*, *6*(9), p.e05000.

Nezis, I.P. and Stenmark, H., 2012. p62 at the interface of autophagy, oxidative stress signaling, and cancer. *Antioxidants & redox signaling*, *17*(5), pp.786-793.

Norris, A.M., Gore, A., Balboni, A., Young, A., Longnecker, D.S. and Korc, M., 2013. AGR2 is a SMAD4-suppressible gene that modulates MUC1 levels and promotes the initiation and progression of pancreatic intraepithelial neoplasia. *Oncogene*, *32*(33), pp.3867-3876.

Oka, O.B. and Bulleid, N.J., 2013. Forming disulfides in the endoplasmic reticulum. *Biochimica et biophysica acta (BBA)-molecular cell research*, *1833*(11), pp.2425-2429.

O'neill, J.R., Pak, H.S., Pairo-Castineira, E., Save, V., Paterson-Brown, S., Nenutil, R., Vojtěšek, B., Overton, I., Scherl, A. and Hupp, T.R., 2017. Quantitative shotgun proteomics unveils candidate novel esophageal adenocarcinoma (EAC)-specific proteins. *Molecular & cellular proteomics*, *16*(6), pp.1138-1150.

Ophuis, R.J., Wijers, M., Bennink, M.B., van de Loo, F.A., Fransen, J.A., Wieringa, B. and Wansink, D.G., 2009. A tail-anchored myotonic dystrophy protein kinase isoform induces perinuclear clustering of mitochondria, autophagy, and apoptosis. *PLoS one*, *4*(11), p.8024.

O'Sullivan, K.E., Phelan, J.J., O'Hanlon, C., Lysaght, J., O'Sullivan, J.N. and Reynolds, J.V., 2014. The role of inflammation in cancer of the esophagus. *Expert review of gastroenterology & hepatology*, *8*(7), pp.749-760.

Pankiv, S., Clausen, T.H., Lamark, T., Brech, A., Bruun, J.A., Outzen, H., Øvervatn, A., Bjørkøy, G. and Johansen, T., 2007. p62/SQSTM1 binds directly to Atg8/LC3 to facilitate degradation of ubiquitinated protein aggregates by autophagy. *Journal of biological chemistry, 282*(33), pp.24131-24145.

Park, S.W., Zhen, G., Verhaeghe, C., Nakagami, Y., Nguyenvu, L.T., Barczak, A.J., Killeen, N. and Erle, D.J., 2009. The protein disulfide isomerase AGR2 is essential for production of intestinal mucus. *Proceedings of the national academy of sciences*, *106*(17), pp.6950-6955.

Park, K., Chung, Y.J., So, H., Kim, K., Park, J., Oh, M., Jo, M., Choi, K., Lee, E.J., Choi, Y.L. and Song, S.Y., 2011. AGR2, a mucinous ovarian cancer marker, promotes cell proliferation and migration. *Experimental & molecular medicine*, *43*(2), pp.91-100.

Patel, P., Clarke, C., Barraclough, D.L., Jowitt, T.A., Rudland, P.S., Barraclough, R. and Lian, L.Y., 2013. Metastasis-promoting anterior gradient 2 protein has a dimeric thioredoxin fold structure and a role in cell adhesion. *Journal of molecular biology*, *425*(5), pp.929-943.

Pavlides, S., Vera, I., Gandara, R., Sneddon, S., Pestell, R.G., Mercier, I., Martinez-Outschoorn, U.E., Whitaker-Menezes, D., Howell, A., Sotgia, F. and Lisanti, M.P., 2012. Warburg meets autophagy: cancer-associated fibroblasts accelerate tumor growth and metastasis via oxidative stress, mitophagy, and aerobic glycolysis. *Antioxidants & redox signaling, 16*(11), pp.1264-1284.

Peinado, H., Lavotshkin, S. and Lyden, D., 2011, April. The secreted factors responsible for pre-metastatic niche formation: old sayings and new thoughts. *Seminars in cancer biology 21*(2), pp.139-146.

Peng, Q., Qin, J., Zhang, Y., Cheng, X., Wang, X., Lu, W., Xie, X. and Zhang, S., 2017. Autophagy maintains the stemness of ovarian cancer stem cells by FOXA2. *Journal of experimental & clinical cancer research, 36*(1), pp.1-12.

Perillo, B., Di Donato, M., Pezone, A., Di Zazzo, E., Giovannelli, P., Galasso, G., Castoria, G. and Migliaccio, A., 2020. ROS in cancer therapy: The bright side of the moon. *Experimental & molecular medicine, 52*(2), pp.192-203.

Persson, S., Rosenquist, M., Knoblach, B., Khosravi-Far, R., Sommarin, M. and Michalak, M., 2005. Diversity of the protein disulfide isomerase family: identification of breast tumor induced Hag2 and Hag3 as novel members of the protein family. *Molecular phylogenetics and evolution*, *36*(3), pp.734-740.

Pohler, E., Craig, A.L., Cotton, J., Lawrie, L., Dillon, J.F., Ross, P., Kernohan, N. and Hupp, T.R., 2004. The Barrett's antigen anterior gradient-2 silences the p53 transcriptional response to DNA damage. *Molecular & cellular proteomics*, *3*(6), pp.534-547.

Presley, J.F., Cole, N.B., Schroer, T.A., Hirschberg, K., Zaal, K.J. and Lippincott-Schwartz, J., 1997. ER-to-Golgi transport visualized in living cells. *Nature*, *389*(6646), pp.81-85.

Ramachandran, V., Arumugam, T., Wang, H. and Logsdon, C.D., 2008. Anterior gradient 2 is expressed and secreted during the development of pancreatic cancer and promotes cancer cell survival. *Cancer research*, *68*(19), pp.7811-7818.

Ponpuak, M., Davis, A.S., Roberts, E.A., Delgado, M.A., Dinkins, C., Zhao, Z., Virgin, H.W., Kyei, G.B., Johansen, T., Vergne, I. and Deretic, V., 2010. Delivery of cytosolic components by autophagic adaptor protein p62 endows autophagosomes with unique antimicrobial properties. *Immunity*, *32*(3), pp.329-341.

Raykhel, I., Alanen, H., Salo, K., Jurvansuu, J., Nguyen, V.D., Latva-Ranta, M. and Ruddock, L., 2007. A molecular specificity code for the three mammalian KDEL receptors. *The journal of cell biology*, *179*(6), pp.1193-1204.

Rogov, V., Dötsch, V., Johansen, T. and Kirkin, V., 2014. Interactions between autophagy receptors and ubiquitin-like proteins form the molecular basis for selective autophagy. *Molecular cell, 53*(2), pp.167-178.

Russell, R.C., Yuan, H.X. and Guan, K.L., 2014. Autophagy regulation by nutrient signaling. *Cell research, 24*(1), pp.42-57.

Schröder, M. and Kaufman, R.J., 2005. ER stress and the unfolded protein response. *Mutation Research/Fundamental and Molecular Mechanisms of Mutagenesis*, *569*(1-2), pp.29-63.

Schroeder, B.W., Verhaeghe, C., Park, S.W., Nguyenvu, L.T., Huang, X., Zhen, G. and Erle, D.J., 2012. AGR2 is induced in asthma and promotes allergen-induced mucin overproduction. *American journal of respiratory cell and molecular biology*, *47*(2), pp.178-185.

Sherman, M.H., Ruth, T.Y., Engle, D.D., Ding, N., Atkins, A.R., Tiriac, H., Collisson, E.A., Connor, F., Van Dyke, T., Kozlov, S. and Martin, P., 2014. Vitamin D receptor-mediated stromal reprogramming suppresses pancreatitis and enhances pancreatic cancer therapy. *Cell*, *159*(1), pp.80-93.

Sukseree, S., László, L., Gruber, F., Bergmann, S., Narzt, M.S., Nagelreiter, I.M., Höftberger, R., Molnár, K., Rauter, G., Birngruber, T. and Larue, L., 2018. Filamentous aggregation of sequestosome-1/p62 in brain neurons and neuroepithelial cells upon Tyr-Cre-mediated deletion of the autophagy gene Atg7. *Molecular neurobiology*, *55*(11), pp.8425-8437.

Sweeter, J.M., Kudrna, K., Hunt, K., Thomes, P., Dickey, B.F., Brody, S.L. and Dickinson, J.D., 2021. Autophagy of mucin granules contributes to resolution of airway mucous metaplasia. *Scientific reports*, *11*(1), pp.1-19.

Taucher, E., Mykoliuk, I., Fediuk, M. and Smolle-Juettner, F.M., 2022. Autophagy, oxidative stress and cancer development. *Cancers*, *14*(7), p.1637.

The ICGC/TCGA Pan-Cancer Analysis of Whole Genomes Network., 2020. Pan-cancer analysis of whole genomes. *Nature*, *578*(7793), pp.82-93.

Thompson, H.G.R., Harris, J.W., Wold, B.J., Lin, F. and Brody, J.P., 2003. p62 overexpression in breast tumors and regulation by prostate-derived Ets factor in breast cancer cells. *Oncogene*, *22*(15), pp.2322-2333.

Thompson, D.A. and Weigel, R.J., 1998. hag-2, the human homologue of thexenopus laeviscement gland gene xag-2, is coexpressed with estrogen receptor in breast cancer cell lines. *Biochemical and biophysical research communications*, *251*(1), pp.111-116.

Tian, S., Hu, J., Tao, K., Wang, J., Chu, Y., Li, J., Liu, Z., Ding, X., Xu, L., Li, Q. and Cai, M., 2018. Secreted AGR2 promotes invasion of colorectal cancer cells via Wnt11-mediated non-canonical Wnt signaling. *Experimental cell research*, *364*(2), pp.198-207.

Tiemann, K., Garri, C., Lee, S.B., Malihi, P.D., Park, M., Alvarez, R.M., Yap, L.P., Mallick, P., Katz, J.E., Gross, M.E. and Kani, K., 2019. Loss of ER retention motif of AGR2 can impact mTORC signaling and promote cancer metastasis. *Oncogene*, *38*(16), pp.3003-3018.

Tian, S.B., Tao, K.X., Hu, J., Liu, Z.B., Ding, X.L., Chu, Y.N., Cui, J.Y., Shuai, X.M., Gao, J.B., Cai, K.L. and Wang, J.L., 2017. The prognostic value of AGR2 expression in solid tumours: a systematic review and meta-analysis. *Scientific reports*, *7*(1), pp.1-10.

Tjalsma, H., Antelmann, H., Jongbloed, J.D., Braun, P.G., Darmon, E., Dorenbos, R., Dubois, J.Y.F., Westers, H., Zanen, G., Quax, W.J. and Kuipers, O.P., 2004. Proteomics of protein secretion by Bacillus subtilis: separating the "secrets" of the secretome. *Microbiology and molecular biology reviews, 68*(2), pp.207-233.

Tsuji, T., Satoyoshi, R., Aiba, N., Kubo, T., Yanagihara, K., Maeda, D., Goto, A., Ishikawa, K., Yashiro, M. and Tanaka, M., 2015. Agr2 mediates paracrine effects on stromal fibroblasts that promote invasion by gastric signet-ring carcinoma cells. *Cancer research, 75*(2), pp.356-366.

Verma, S., Salmans, M.L., Geyfman, M., Wang, H., Yu, Z., Lu, Z., Zhao, F., Lipkin, S.M. and Andersen, B., 2012. The estrogen-responsive Agr2 gene regulates mammary epithelial proliferation and facilitates lobuloalveolar development. *Developmental biology*, *369*(2), pp.249-260.

Vitale, A. and Denecke, J., 1999. The endoplasmic reticulum—gateway of the secretory pathway. *The plant cell*, *11*(4), pp.615-628.

Vitello, E.A., Quek, S.I., Kincaid, H., Fuchs, T., Crichton, D.J., Troisch, P. and Liu, A.Y., 2016. Cancer-secreted AGR2 induces programmed cell death in normal cells. *Oncotarget, 7*(31), p.49425.

Wang, M., Zhu, J., Lubman, D.M. and Gao, C., 2019. Aberrant glycosylation and cancer biomarker discovery: a promising and thorny journey. *Clinical Chemistry and Laboratory Medicine, 57*(4), pp.407-416.

Ward, J.F., Evans, J.W., Limoli, C.L. and Calabro-Jones, P., 1987. Radiation and hydrogen peroxide induced free radical damage to DNA. *British journal of cancer*, *55*(8), pp.105-112

Whitwell, H.J., Worthington, J., Blyuss, O., Gentry-Maharaj, A., Ryan, A., Gunu, R., Kalsi, J., Menon, U., Jacobs, I., Zaikin, A. and Timms, J.F., 2020. Improved early detection of ovarian cancer using longitudinal multimarker models. *British journal of cancer*, *122*(6), pp.847-856.

Worfolk, J.C., Bell, S., Simpson, L.D., Carne, N.A., Francis, S.L., Engelbertsen, V., Brown, A.P., Walker, J., Viswanath, Y.K. and Benham, A.M., 2019. Elucidation of the AGR2 interactome in esophageal adenocarcinoma cells identifies a redox-sensitive chaperone hub for the quality control of MUC-5AC. *Antioxidants & redox signaling*, *31*(15), pp.1117-1132.

Wu, J., Chen, S., Liu, H., Zhang, Z., Ni, Z., Chen, J., Yang, Z., Nie, Y. and Fan, D., 2018. Tunicamycin specifically aggravates ER stress and overcomes chemoresistance in multidrug-resistant gastric cancer cells by inhibiting N-glycosylation. *Journal of Experimental & Clinical Cancer Research*, *37*(1), pp.1-12.

Wu, Z., Newstead, S. and Biggin, P.C., 2020. The KDEL trafficking receptor exploits pH to tune the strength of an unusual short hydrogen bond. *Scientific Reports, 10*(1), p.16903.

Yoon, Y.H., Cho, K.S., Hwang, J.J., Lee, S.J., Choi, J.A. and Koh, J.Y., 2010. Induction of lysosomal dilatation, arrested autophagy, and cell death by chloroquine in cultured ARPE-19 cells. *Investigative ophthalmology & visual science*, *51*(11), pp.6030-6037.

Yun, C.W. and Lee, S.H., 2018. The roles of autophagy in cancer. *International journal of molecular sciences*, *19*(11), p.3466.

Zacherl, S., La Venuta, G., Müller, H.M., Wegehingel, S., Dimou, E., Sehr, P., Lewis, J.D., Erfle, H., Pepperkok, R. and Nickel, W., 2015. A direct role for ATP1A1 in unconventional secretion of fibroblast growth factor 2. *Journal of biological chemistry*, *290*(6), pp.3654-3665.

Zhang, J.S., Gong, A., Cheville, J.C., Smith, D.I. and Young, C.Y., 2005. AGR2, an androgen-inducible secretory protein overexpressed in prostate cancer. *Genes, chromosomes and cancer*, *43*(3), pp.249-259.

Zhang Y, Forootan SS, Liu D, Barraclough R, Foster CS, Rudland PS, Ke Y., 2007. Increased expression of anterior gradient-2 is significantly associated with poor survival of prostate cancer patients. *Prostate cancer and prostatic diseases*, *10*(3), pp.293-300.

Zheng, W., Rosenstiel, P., Huse, K., Sina, C., Valentonyte, R., Mah, N., Zeitlmann, L., Grosse, J., Ruf, N., Nürnberg, P. and Costello, C.M., 2006. Evaluation of AGR2 and AGR3 as candidate genes for inflammatory bowel disease. *Genes & immunity*, *7*(1), pp.11-18.

Zhu, H., Lam, D.C.L., Han, K.C., Tin, V.P.C., Suen, W.S., Wang, E., Lam, W.K., Cai, W.W., Chung, L.P. and Wong, M.P., 2007. High resolution analysis of genomic aberrations by metaphase and array comparative genomic hybridization identifies candidate tumour genes in lung cancer cell lines. *Cancer letters*, *245*(1-2), pp.303-314.

Zmijewski, J.W., Banerjee, S., Bae, H., Friggeri, A., Lazarowski, E.R. and Abraham, E., 2010. Exposure to hydrogen peroxide induces oxidation and activation of AMP-activated protein kinase. *Journal of biological chemistry*, *285*(43), pp.33154-33164.